Citation: Pujol-Solà, N., Casas, J.M., Proenza, J., Blanco-Quintero, I., Druguet, E., Liesa, M., Román-Alpiste, M., Álvaro, J., 2022. Cadomian metabasites of the Eastern Pyrenees revisited. Geologica Acta, 20.13, 1-26, I-IV.
DOI: 10.1344/GeologicaActa2022.20.13

geologica acta

Cadomian metabasites of the Eastern Pyrenees revisited

Núria Pujol-Solà[1] Josep Maria Casas[2] Joaquín A. Proenza[1] Idael F. Blanco-Quintero[3] Elena Druguet[4] Montserrat Liesa[1] Manuel J. Román-Alpiste[5] J. Javier Álvaro[6]

[1]Departament de Mineralogia, Petrologia i Geologia Aplicada. Facultat de Ciències de la Terra, Universitat de Barcelona
Carrer Martí i Franquès, s/n, 08028, Barcelona, Spain. Pujol-Solà E-mail: npujolsola@ub.edu Proenza E-mail: japroenza@ub.edu
Liesa E-mail: mliesa@ub.edu

[2]Departament de Dinàmica de la Terra i de l'Oceà. Facultat de Ciències de la Terra, Universitat de Barcelona
Carrer Martí i Franquès, s/n, 08028, Barcelona, Spain. E-mail: casas@ub.edu

[3]Departamento de Ciencias de la Tierra y del Medio Ambiente. Facultad de Ciencias, Universidad de Alicante
Carretera de San Vicente del Raspeig s/n, 03690, Alicante, Spain. E-mail: if.blanco@ua.es

[4]Departament de Geologia, Universitat Autònoma de Barcelona
08193 Bellaterra, Spain. E-mail: elena.druguet@uab.cat

[5]Instituto Andaluz de Ciencias de la Tierra (CSIC-UGR)
Avda. de las Palmeras 4, E-18100 Armilla, Granada, Spain. E-mail: mj.roman@csic.es

[6]Instituto de Geociencias (CSIC-UCM)
Dr. Severo Ochoa 7, 28040 Madrid, Spain. E-mail: jj.alvaro@csic.es

ABSTRACT

This study presents a new geochemical, petrological, and geochronological U-Pb dataset from Ediacaran metabasites and associated rocks of the Canigó and Cap de Creus massifs, Eastern Pyrenees. Metabasites are composed of calcic amphibole + plagioclase + chlorite + epidote ± quartz plus titanite + apatite + ilmenite ± biotite ± rutile as accessory phases and show relict igneous textures. Peak pressure-temperature determinations share common conditions, ranging 452-482ºC and 5.2-7.7kbar, which suggest Barrovian-type metamorphism, most likely related to a collisional setting. The metabasites correspond to evolved basaltic rocks (Mg#<0.55) with moderate TiO_2 content (up to 2.08wt.%) and relatively low Cr (43-416ppm). The rocks are moderately enriched in Light Rare Earth Elements (LREE) relative to Heavy Rare Earth Elements (HREE) (average $(La/Lu)_n$ of 2.7) and the N-MORB normalized multi-element patterns show negative slopes, with prominent negative Nb anomalies ($(Nb/La)_{NMORB}$=0.33–0.78). These variations are akin to island arc tholeiites generated in back-arc basins and to other metabasites described in the Eastern Pyrenees with a putative Ediacaran age, and they differ from the Ordovician tholeiitic metabasites from the Canigó massif, which derived from a contaminated E-MORB source. The positive $\varepsilon_{Nd(T)}$ values (0.82-3.05) of the studied metabasites preclude a notable contribution from an older continental crust. Detrital zircon U-Pb dating Laser Ablation-Inductively Coupled Plasma-Mass Spectrometry (LA-ICP-MS) of one chlorite-rich schist sample in contact with the metabasites from the Canigó massif yielded a main peak at ca. 632Ma and apparent maximum age of deposition at ca. 550Ma. We argue that the Cadomian metabasites from the Pyrenees formed during back-arc extension in the continental margin of Gondwana and were later affected by (probably early Variscan) medium-P metamorphism before the Low-Pressure High-Temperature (LP-HT) metamorphism classically described in the Pyrenees.

KEYWORDS **Pan-African. Cadomian. Inherited zircon. Peri-Gondwanan. Iberian Massif.**

INTRODUCTION

Ediacaran mafic magmatic rocks related to the Pan-African collisional orogen (~790-605Ma in the Anti-Atlas) and Cadomian accretional orogen (~590-550Ma in SW Europe) have been extensively described in the north-western margin of Gondwana, exposed in several areas of the European Variscan Belt (Arenas *et al.*, 2018; Gutiérrez-Alonso *et al.*, 2004; Rubio-Ordóñez *et al.*, 2015; Sánchez-Lorda *et al.*, 2014, 2016 and references therein). Ediacaran magmatic rocks are the only evidence of the Cadomian orogenic event in areas far from the main sutures, where Cadomian-related deformation and metamorphism are absent, such as in the basement rocks of the Eastern Pyrenees (Casas *et al.*, 2015; Castiñeiras *et al.*, 2008; Mezger, 2010; Navidad and Carreras, 1995; Padel *et al.*, 2018a) or in the core of other massifs involved in the Alpine-Himalayan orogenic system (Abbo *et al.*, 2015; Bendokht *et al.*, 2021; Fiannacca *et al.*, 2013; Micheletti *et al.*, 2007; Williams *et al.*, 2012; Yilmaz Şahin *et al.*, 2013). In general, the described Cadomian magmatic events are associated with the later stages of a long-lived active margin that resulted from the subduction of a former *peri*-Gondwanan Ocean (Prototethys or Iapetus?) under Gondwana (*e.g.* Kroner and Stern, 2005; Nance *et al.*, 2010).

Despite the efforts on clarifying the age and the tectonic settings of the metabasite rocks exposed in the Pyrenees (Casas *et al.*, 2015; Castiñeiras *et al.*, 2008; Navidad and Carreras, 1995; Padel *et al.*, 2018a), there is still controversy regarding their paleogeographic location and geodynamic meaning during the Cadomian orogeny and so far, have been subsequently less studied compared with other areas (see von Raumer *et al.*, 2015). Recently, Padel *et al.* (2018a) interpreted the Ediacaran metabasites in the Eastern Pyrenees as formed due to the emplacement of tholeiitic magmas linked to an extensional regime. According to these authors, such extensional event preceded the Cadomian felsic and calc-alkaline more extensive magmatism attributed to the arc-related final stage of the Cadomian orogen. Padel *et al.* (2018a) also compared the magmatic geological record in the Eastern Pyrenees with that from the Serie Negra Group of the Ossa-Morena Zone, which is interpreted as an oceanic environment with island-arc affinity linked to fore- and back-arc basins (Sánchez-Lorda *et al.*, 2014, 2016). However, other authors suggest that the Cadomian mafic and felsic magmatic episodes in the Eastern Pyrenees may be coeval (Álvaro *et al.*, 2018; Ayora and Casas, 1986; Navidad and Carreras, 2002).

The purpose of this study is to provide more precise information on the petrogenesis of the late Neoproterozoic basic magmatism recorded in the basement rocks of the Pyrenees and to clearly differentiate the Ediacaran vs. Ordovician mafic magmatic pulses recorded in these rocks. We present new geochemical and petrological, U-Pb zircon geochronological, and Sr-Nd isotopic data of the Eastern Pyrenees metabasites and associated rocks to further constrain their origin and age and, as a result, to get a better understanding of the geodynamic evolution of the basement rocks of the Pyrenees along the Gondwana margin during the Ediacaran-Cambrian transition. In addition, we discuss their P-T paths in order to constrain the metamorphism undergone by the studied mafic rocks.

GEOLOGICAL SETTING

The Pyrenees is an E-W trending Alpine belt formed between the Late Cretaceous and the Miocene by the convergence between the Iberian and European plates (Muñoz, 1992). Due to the tectonic stacking of several Alpine thrust-sheets, pre-Variscan basement rocks form a large strip in the core of the cordillera and provide evidence of Cadomian, Sardic, and Variscan magmatic episodes (Casas *et al.*, 2010, 2015; Castiñeiras *et al.*, 2008; Cocherie *et al.*, 2005; Liesa *et al.*, 2021; Martínez *et al.*, 2016; Navidad *et al.*, 2010; Padel *et al.*, 2018a; Pereira *et al.*, 2014). The Ediacaran succession (Casas and Palacios, 2012; Castiñeiras *et al.*, 2008) is a thick (up to 3000?m) unfossiliferous metasedimentary series (Canaveilles Group and lateral equivalents; Padel *et al.*, 2018b), composed of metapelites and metagreywackes interbedded with numerous layers of marbles, quartzites, and calc-silicates cut by orthogneiss derived from Ordovician protoliths (Castiñeiras *et al.*, 2008; Casas *et al.*, 2010; Navidad *et al.*, 2018). The study area is located on the southern flank of the Canigó massif and on the Cap de Creus massif (Fig. 1), where this lower metasedimentary series crops out extensively.

Variscan deformation events are also linked to regional metamorphic conditions (Guitard, 1970; Muñoz, 1992; Ribeiro *et al.*, 2019; Zwart, 1979; and references therein). The main Variscan structure is a pervasive S_1 foliation present at all structural levels. S_1 foliation is heterogeneously affected by later D_2 and D_3 folds with associated axial planar foliations, developing into broadly E-W to NW-SE orientation. The resulting main structure is characterized by dome-shaped antiforms (generally cored by orthogneisses) bounded by synforms formed by upright folded metasediments with a steeply dipping axial plane foliation (Carreras and Capellà, 1994; Carreras *et al.*, 1996), thus, suggesting that the main Variscan phase was contractional (Carreras and Capellà, 1994; Matte and Mattauer 1987).

Metamorphic zones linked to a Low-Pressure High-Temperature (LP-HT) metamorphism (broadly coeval with the Variscan D_2 event) are developed concentrically around

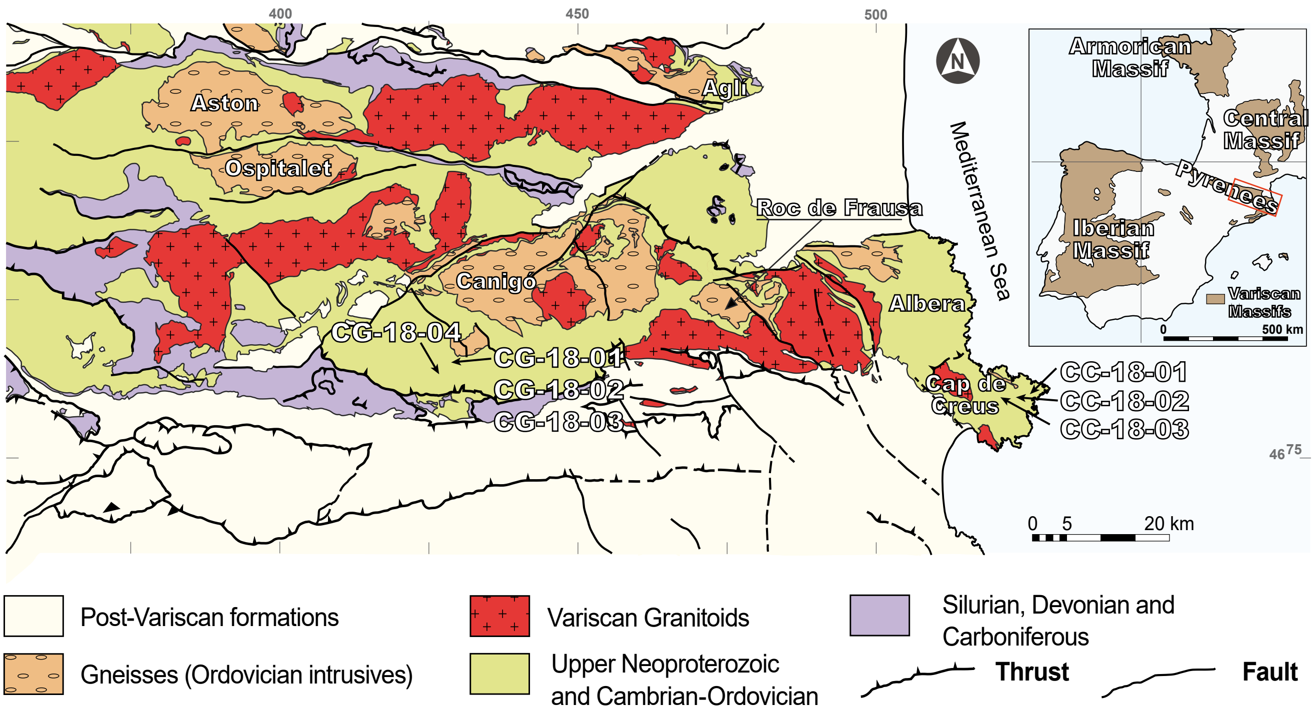

FIGURE 1. Simplified geological map of the Eastern Pyrenees with the location of the Canigó and Cap de Creus massifs, and the location of the studied samples. The inset in the upper right shows the location of the Pyrenees in southwestern Europe. Modified from Casas *et al.* (2015).

the antiforms (Gibson, 1989; Guitard, 1965; Guitard *et al.*, 1996; Liesa and Carreras, 1989; Soula, 1982; Zwart, 1962, 1979). Medium to high-grade rocks (cordierite-andalusite and sillimanite zones) and local migmatites are present in the inner parts, while the external parts of the antiforms are occupied by low-grade rocks (chlorite-muscovite and biotite zones). Late folds and shear zones affected the main foliation, and local retrograde greenschist facies metamorphism developed along mylonitic bands (Carreras and Casas, 1987; Carreras, 2001; Carreras and Druguet, 2014).

In the Cap de Creus, the deeper stratigraphic and highest metamorphic rocks are located towards the NE, structurally covered by a continuous series of progressively lower metamorphic grade rocks in the upper stratigraphic sequences (Druguet, 2001). Reche *et al.* (1996) estimated P-T conditions around 550-570ºC and 2.5-3.6kbar for the upper part of the cordierite-andalusite zone and between 3.9-6.5kbar and 590-720ºC for the sillimanite - K feldspar zone.

In the Canigó massif, P-T conditions of 4.6-6kbar and 450-530ºC were estimated for the biotite zone (Ayora *et al.*, 1993) and ~6.5kbar and 550°C (de Marien *et al.*, 2019) coeval with the development of the main foliation. In the andalusite-cordierite zone, the presence of staurolite wrapped by andalusite and cordierite indicates a previous medium-pressure stage followed by lower-pressure metamorphism (Castro *et al.*, 2002; Gibson, 1992; Martínez and Rolet, 1988). For the sillimanite zone, peak temperatures reached 725±25ºC at 4.5±0.5kbar (Gibson and Bickle, 1994).

The Cadomian cycle and the Ediacaran metabasites in the Pyrenees

The Canigó massif

The presence of pre-Variscan igneous rocks in the basement rocks of the Pyrenees was first reported in the Canigó massif by Guitard and Laffitte (1956) and Cavet (1957). These authors described metavolcanic acidic rocks with a porphyritic texture, known as *gneiss granulé* (granular gneiss) located in the lower part of the metasedimentary Canaveilles Group. Later, Guitard (1970), Casas *et al.* (1986), Ayora and Casas (1986) and Navidad and Carreras (2002) described greenschists and amphibolites derived from basaltic lava flows, diabasic dikes, and gabbro bodies mainly located in the lower and middle parts of the succession (Fig. 2). According to Ayora and Casas (1986) and Navidad and Carreras (2002), the close proximity of metavolcanic acidic and basic rocks may indicate that this bimodal magmatism could be coeval.

On the southern flank of the massif, Casas *et al.* (2015) provided radiometric ages ranging from 575 to 568Ma for

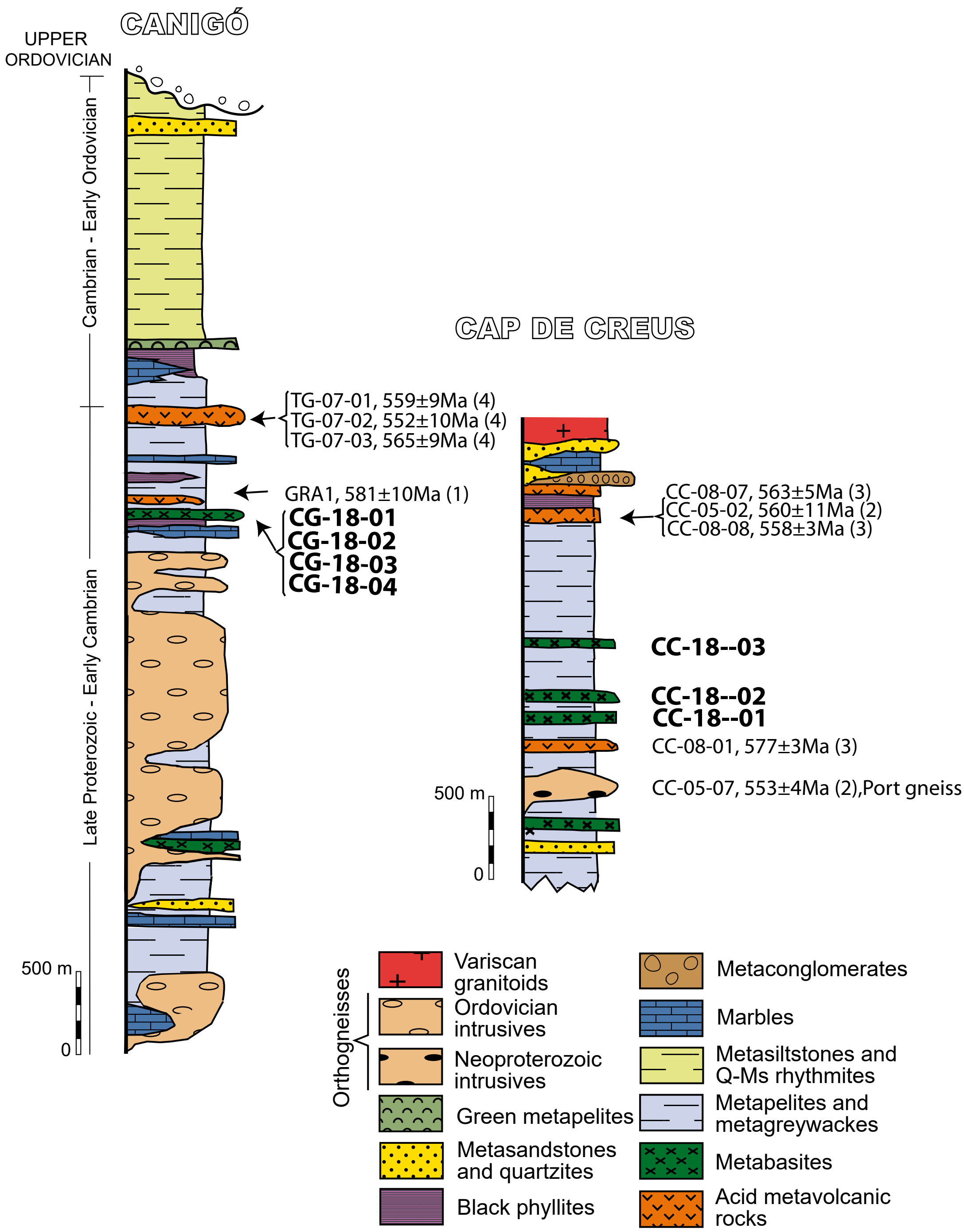

FIGURE 2. Synthetic logs of pre-Upper Ordovician rocks in the Canigó and Cap de Creus massifs with the location of the studied samples and the previous geochronological data related to Cadomian magmatism: 1) Cocherie *et al.* (2005); 2) Castiñeiras *et al.* (2008); 3) Casas *et al.* (2015); 4) Casas *et al.* (2015) recalculated after Padel *et al.* (2018a). Stratigraphic data from Guitard (1970), Santanach (1972), Ayora and Casas (1986) and Losantos *et al.* (1997).

feldspathic metaignimbrites collected near the Tregurà village, in an area where the metavolcanic rocks attain their maximum thickness (up to 500m). The geochemistry of the felsic rocks indicates that they were formed in a back-arc environment, and they record a fragment of a long-lived subduction-related magmatic arc (620-520Ma) in the active northwestern Gondwana margin. In the same area, Padel *et al.* (2018b) proposed an updated revision of the Ediacaran-Lower Ordovician stratigraphic framework and subdivided the succession topped by the Sardic unconformity into the Canaveilles and Jujols groups. According to these authors, the main volcanic activity is located in the upper part of the Canaveilles Group (Fabert and Finestrelles members of the Pic de la Clape Formation) crossing the Ediacaran-Terreneuvian boundary interval. Padel *et al.* (2018b) recalculated the age of the Tregurà volcanic rocks (ca. 565-552Ma) and proposed that the metabasites reflect the emplacement of tholeiitic magmatism linked to Ediacaran extensional conditions, whereas predominant subsequent intermediate and acid magmatic rocks should represent Cadomian magmatic events.

The Cap de Creus massif

In the Cap de Creus massif, the lower parts of the equivalent Canaveilles Group are mainly made up of a ca. 800m thick monotonous alternation of metagreywackes, with subordinate metapelites and discontinuous bands of plagioclase-amphibole rocks, banded quartzites, and marbles. Acidic metatuffs are mainly interstratified at the top of this succession, whereas metabasites crop out at its bottom and middle parts (Fig. 2; Navidad and Carreras, 1995). Metatuffs are interbedded with kerogenous black slates and marbles and are derived from late Ediacaran Al-rich calc-alkaline rhyolites and rhyodacites (Navidad and Carreras, 1995). They yield U-Pb zircon ages ranging from ca. 577Ma at the base of the succession (Casas *et al.*, 2015), to ca. 560Ma, (Castiñeiras *et al.*, 2008), ca. 563Ma, and ca. 558Ma (Casas *et al.*, 2015) at its top. Metabasites are derived from gabbro-dolerite intrusions and basaltic lens-shaped bodies and, till now, no radiometric age has been obtained from these rocks.

In contrast to other Pyrenean massifs (Canigó, Albera, Roc de Frausa, and Aston-Ospitalet), no large augengneiss bodies derived from Ordovician plutonic rocks occur in the Cap de Creus massif. In contrast, a 200m thick subvolcanic orthogneiss body (the so-called Port gneiss; Carreras and Ramírez, 1984) crops out at the bottom of the succession. Its protolith corresponds to a small intrusion of quartz-monzonite yielding a ca. 553Ma U-Pb radiometric age (Castiñeiras *et al.*, 2008) (Fig. 2). This gneiss can be considered as the plutonic equivalent of the metavolcanic rocks mainly located in the upper part of the succession. Its radiometric age is similar to the protolith age of other gneissic bodies located at similar stratigraphic positions, such as the Mas Blanc gneiss in the Roc de Frausa massif (ca. 560Ma; Castiñeiras *et al.*, 2008), the Laparan orthogneiss in the Aston massif (ca. 545Ma; Mezger and Gerdes, 2016), and the Belesta gneiss in the Aglí massif (ca. 542Ma; Tournaire Guille *et al.*, 2019).

In summary, the Canigó and Cap de Creus massifs of the Eastern Pyrenees provide evidence of a stepwise succession of Ediacaran-Terreneuvian magmatic events lasting 30m.y. Felsic rocks clearly predominate, which is common for the magmatism related to the Cadomian orogeny (Villaseca *et al.*, 2022 and references therein), and subsidiary mafic bodies have received different interpretations with no conclusive radiometric ages.

SAMPLES AND ANALYTICAL METHODS

Four localities from the Canigó massif near the Queralbs village were sampled, three of them between La Farga and Daió power station and one on the Queralbs-Fontalba road (see locations in Table 1; Figs. 1; 2). Two samples are metabasites (CG-18-01 and CG-18-04) and two samples are chlorite-rich schists (CG-18-02, CG-18-03) in close contact with the metabasites. Metabasites from the Cap de Creus were sampled in 3 localities: east of Mas d'en Melos, north of the Bufadors area, and in the Serrat de Conilleres, the three located between Cadaqués and Port de la Selva (see locations in Table 1; Figs. 1; 2).

In the Canigó massif, metabasites occur as lens-shaped half-meter to 3m-wide and about 10 to 100m-long bodies (Fig. 3A-B), with NW-SE trending direction and steep to sub-vertical dips (Table 1), sub-parallel to the main foliation in the country rocks. Metabasites occur in the lower part of the succession, in the vicinity of felsic metavolcanics (Fig. 2).

In the Cap de Creus massif, felsic bodies are scarce in the lower and middle part of the succession, where metabasites are abundant (Fig. 2). Metabasites also occur as lens-shaped bodies sub-parallel to the E-W to NW-SE trending main Variscan foliation, which affects the metabasite lenses (Fig. 3C-D) but may also wrap around the larger, more competent bodies. The larger body around the Bufadors area is about 200m wide and 1km long.

Unaltered representative metabasites (CG-18-01, CG-18-04, CC-18-01, CC-18-02, CC-18-03) and one chlorite-rich schist (CG-18-02) were crushed in a jaw crusher and powdered using a tungsten carbide disk mill (~1.5kg per sample). The powder was sieved using various mesh sizes disposable plastic sieves and the fractions 75-100μm and 100-125μm were separated first using a Frantz™ isodynamic separator and the non-magnetic fractions were hydroseparated at the Hydroseparation Lab (Universitat de Barcelona; http://www.hslab-barcelona.com/). The obtained grains were mounted as polished (1μm diamond paste) monolayers on resin blocks (SimpliMet 1000). For details of the procedure see Aigslperger *et al.* (2015).

Polished thin sections and monolayers were studied by optical and electron microscopy using a Quanta 200 FEI XTE 325/D8395 Scanning Electron Microscope (SEM) equipped with an INCA Energy 250 EDS microanalysis system and a JEOL JSM-7100 field-emission SEM at

TABLE 1. Studied samples, classification, location, and dip and dip direction of the main foliation

Sample	Rock type	Sampling site	Dip	Dip Dir.	Latitude	Longitude
CG-18-01	Metabasalt	Canigó massif, La Farga	82	218	42.35856987	2.17237632
CG-18-02	Chlorite-rich schist	Canigó massif, La Farga	71	53	42.35849162	2.17211774
CG-18-03	Chlorite-rich schist	Canigó massif, La Farga	82	225	42.35823539	2.17197935
CG-18-04	Metagabbro	Canigó massif, Fontalba road	68	19	42.35494545	2.16267494
CC-18-01	Metagabbro	Cap de Creus massif. E Mas d'en Melos	56	59	42.31122364	3.26784228
CC-18-02	Metagabbro	Cap de Creus massif. N Bufadors	75	62	42.30810586	3.24797851
CC-18-03	Metabasalt	Cap de Creus massif, Serrat de Conilleres	35	360	42.30689786	3.22657767

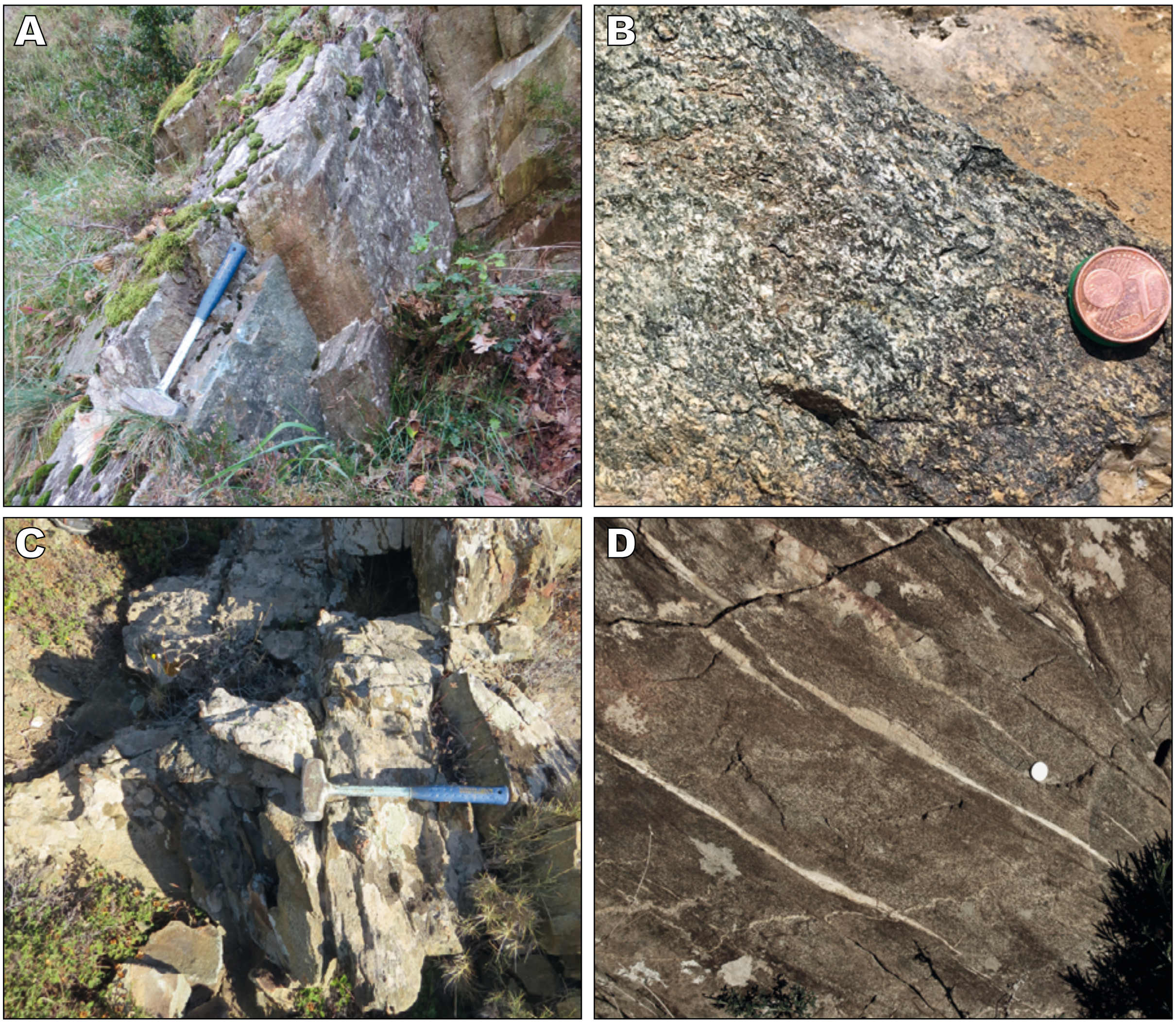

FIGURE 3. Field images of the studied samples. A-B) Metabasites from the Canigó massif. C-D) Metabasites from the Cap de Creus massif. Photograph D courtesy of J. Carreras.

the Centres Científics i Tecnològics de la Universitat de Barcelona (CCiTUB). Operating conditions were 15-20kV accelerating voltage and 5nA in BackScattered Electron (BSE) mode. Monolayers were studied uncoated under low-vacuum conditions. Semiquantitative compositions of the mineral assemblage were determined by X-ray Energy Dispersive System (EDS) analysis.

Quantitative ElectronProbe MicroAnalyses (EPMA) on amphibole, plagioclase, chlorite, epidote, titanite, ilmenite, rutile, magnetite and biotite were also conducted at the CCiTUB using a five-channel JEOL JXA-8230 operating in Wavelength-Dispersive Spectroscopy (WDS) mode. The analytical conditions were 15-20kV accelerating voltage, 10-20nA beam current, 1-2μm beam diameter, and 10-20s counting time per element, using WDS detectors and XPP matrix correction (Pouchou and Pichoir, 1991). The measurements and the calibrations were performed using the following natural and synthetic standards: diopside (Si), kyanite (Al), Cr_2O_3 (Cr), rutile (Ti), periclase (Mg), albite (Na), Fe_2O_3 (Fe), rhodonite (Mn), NiO (Ni), wollastonite (Ca), orthoclase (K), NaCl (Cl) and CaF (F). Representative analyses are given in Appendix I. Amphibole compositions were normalized following the procedures of Leake *et al.* (1997) and Fe^{3+} was estimated after the method of Schumacher (in Leake *et al.*, 1997), although they were revised by the newer scheme of Hawthorne *et al.* (2012). Epidote and feldspar were normalized to 12.5 and 8 oxygens, respectively, and Fe_{total}=Fe^{3+}. Chlorite was normalized to 28 oxygen and Fe_{total}=Fe^{2+}. Atoms per formula unit are abbreviated as apfu. Atomic Mg/(Mg+Fe^{2+}) of minerals is expressed as Mg-number (Mg#). Mineral abbreviations are after Whitney and Evans (2010).

Bulk rock geochemical and isotopic analyses were performed at the Centro de Instrumentación Científica from the Universidad de Granada (CIC-UGR). Secondary veins and alteration rims were carefully removed by sawing before crushing. Sample powders were obtained using a tungsten carbide disk mill. Major-element concentrations were obtained by X-ray Fluorescence (XRF) spectrometry on glass beds using a Philips PV1404 spectrometer. Precision was better than ±1.5% for a concentration of 10wt.%. Zr was determined by XRF on pressed powder pellets, with a precision better than ±4% at 100ppm concentration. Further detail on the analytical technique can be found in Lázaro *et al.* (2015). Trace elements were analyzed by Inductively Coupled Plasma Mass Spectrometry (ICP-MS). Procedural blanks and international standards PMS, WSE, UBN, BEN, BR, and AGV (Govindaraju, 1994) were run as unknowns during analytical sessions. Precision was better than ±2% and ±5% for analyte concentrations of 50 and 5ppm, respectively. Further detail in Lázaro *et al.* (2015). Major and trace elements of six metabasites from the Canigó (CG-18-01A, CG-18-01B, CG-18-04) and Cap de Creus (CC-18-01, CC-18-02, CC-18-03) massifs are listed in Table 2.

The same metabasite samples analyzed for whole-rock geochemistry were analyzed for Sr and Nd isotopes at the CIC-UGR. Powders were digested using ultra-clean reagents, chromatographically separated with ion-exchange resins in a clean room and analyzed by Thermal Ionization Mass Spectrometry (TIMS) in a Finnigan Mat 262 spectrometer. Normalization values were ^{86}Sr/^{88}Sr=0.1194 and ^{146}Nd/^{144}Nd=0.7219 and blanks were 0.6 and 0.09ng for Sr and Nd respectively. The external precision (2σ; Govindaraju *et al.*, 1994) was better than 0.0011% for ^{87}Sr/^{86}Sr, and 0.0018% for ^{143}Nd/^{144}Nd. The internal precision was estimated on the average of the standards NIST-987 for Sr with a mean ^{87}Sr/^{86}Sr=0.710249±0.0003% and Jndi-1 (Tanaka *et al.*, 2000) for Nd with a mean ^{143}Nd/^{144}Nd=0.512123±0.0006%. ^{87}Rb/^{86}Sr and ^{147}Sm/^{144}Nd were directly determined by ICP-MS according to the method developed by Montero and Bea (1998), with a precision better than 1.2% and 0.9% (2σ) respectively. The analyses are given in Table 3.

Zircon grains were found in the mineral concentrates of only one chlorite-rich schist (CG-18-02). U/Pb isotopes of zircon were measured *in situ* on polished monolayers by an inductively coupled mass spectrometer Agilent 8800 QQQ ICP-MS interfaced to a laser ablation extraction line Photon Machines Analyte Excite 193 at the Andalchron lab (Instituto Andaluz de Ciencias de la Tierra, CSIC-UGR, Granada). Ablation conditions were set up to get the maximum sensibility on analysis, minimize interactions and interferences, and get accurate location analysis, avoiding mixed areas, fractures, and irregularities over the ablated area. 81 analyses on zircon grains from 2 different monolayers were performed with a spot size of 40μm, fluence of 8J/cm^2, static spot ablation mode, and automatic driven positioning. The masses measured and integration times were 0.38s (206), 0.5s (207), 0.2s (208), 0.15s (232), and 0.28s (238). 91500 zircon (Wiedenbeck *et al.*, 1995) was used as primary reference material for every four analyses of unknows and the Plesovice zircon (Sláma *et al.*, 2008) for secondary/validation. Data were subsequently reduced using Igor Pro Iolite 3.5 software (Paton *et al.*, 2011) and Isoplot R for data presentation. The obtained results are shown in Table VI, appendix I.

P-T conditions were determined with the average P-T method using the software THERMOCALC version 3.33 and dataset 5.5 (Powell and Holland, 1994; Holland and Powell, 1998). An H_2O-fluid was included in all the assemblages. The activities and activity uncertainties of each endmember included in the calculations were obtained with the software AX (Holland and Powell, unpublished). Endmembers with very low activities (<0.0001) were

TABLE 2. Whole-rock major and trace element data of the studied metabasites from the Canigó and Cap de Creus massifs

Sample	CG-18-01A	CG-18-01B	CG-18-04	CC-18-01	CC-18-02	CC-18-03
Region	Canigó	Canigó	Canigó	Cap de Creus	Cap de Creus	Cap de Creus
Rock type	Metabasalt	Metabasalt	Metagabbro	Metagabbro	Metagabbro	Metabasalt
SiO_2 (wt.%)	44.95	44.93	48.51	50.93	52.84	52.16
TiO_2	1.01	0.98	1.39	1.12	2.08	1.58
Al_2O_3	14.98	15.02	17.74	13.96	12.26	14.14
Fe_2O_{3T}	11.54	11.63	9.56	10.69	15.26	12.40
MnO	0.18	0.19	0.12	0.17	0.22	0.20
MgO	11.08	11.10	5.69	7.41	5.07	5.56
CaO	9.10	9.13	9.30	10.65	7.21	7.89
Na_2O	2.21	2.19	3.83	2.89	3.72	4.25
K_2O	0.03	0.03	0.20	0.32	0.23	0.20
P_2O_5	0.11	0.11	0.16	0.09	0.17	0.16
LOI	4.22	3.97	3.01	1.02	0.23	0.72
Total	99.41	99.28	99.51	99.25	99.29	99.26
Li (ppm)	43	44	35	8	7	13
Rb	1.3	1.2	5.9	6.5	6.1	4.6
Cs	0.19	0.18	0.47	0.51	1.58	0.42
Be	0.75	0.74	0.80	0.62	1.13	1.02
Sr	268	262	279	202	270	332
Ba	21	14	53	91	228	571
Sc	27	26	41	51	53	44
V	153	148	235	280	577	357
Cr	406	417	341	247	43	123
Co	190	244	72	120	136	125
Ni	221	218	59	47	14	35
Cu	16	15	120	53	12	63
Zn	96	94	82	89	96	94
Ga	15	15	20	17	20	20
Y	21	20	23	27	39	36
Nb	4	4	7	3	4	4
Ta	0.92	1.13	0.61	0.50	0.59	0.57
Zr	70	73	91	71	114	108
Hf	0.50	0.72	1.18	0.67	0.74	0.89
Mo	6	8	6	8	9	8
Sn	0.95	0.95	1.08	1.13	2.04	1.76
Tl	0.02	0.01	0.03	0.05	0.07	0.04
Pb	12	11	5	5	2	10
U	0.21	0.20	0.34	0.34	0.33	0.68
Th	0.84	0.80	1.51	1.25	1.90	2.17
La	6.3	6.0	9.5	7.4	7.6	13.4
Ce	13.9	13.4	20.1	15.8	20.0	30.1
Pr	1.88	1.81	2.56	2.11	2.97	4.02
Nd	9.05	8.61	11.69	10.10	15.04	18.27
Sm	2.50	2.45	3.16	2.93	4.57	4.80
Eu	1.08	0.97	1.17	1.18	1.72	1.70
Gd	2.94	2.79	3.54	3.57	5.28	5.33
Tb	0.51	0.49	0.62	0.66	0.96	0.91
Dy	3.13	3.13	3.72	4.16	6.62	5.99
Ho	0.71	0.69	0.79	0.94	1.47	1.33
Er	1.88	1.85	2.07	2.64	4.13	3.63
Tm	0.29	0.29	0.31	0.40	0.60	0.53
Yb	1.76	1.72	1.89	2.52	3.82	3.44
Lu	0.24	0.24	0.26	0.37	0.57	0.50

TABLE 3. Rb-Sr and Sm-Nd isotopic data for the studied metabasites. εNd calculated for 580Ma, Nd model ages after DePaolo (1981), decay constant for ^{147}Sm= 6.54•10-12 y^{1} (Lugmair and Martí, 1978), and present-day CHUR parameters: $^{147}Sm/^{144}Nd$= 0.1967; $^{143}Nd/^{144}Nd$= 0.512638 (Jacobsen and Wasserburg, 1980)

Sample	CG-18-01A	CG-18-01B	CG-18-04	CC-18-01	CC-18-02	CC-18-03
Region	Canigó	Canigó	Canigó	Cap de Creus	Cap de Creus	Cap de Creus
Rock type	Metabasalt	Metabasalt	Metagabbro	Metagabbro	Metagabbro	Metabasalt
Rb(ppm)	1.03	0.94	6.52	6.07	6.18	3.70
Sr(ppm)	307.6	307.4	226.5	325.6	315.1	387.2
$^{87}Rb/^{86}Sr$	0.0096	0.0089	0.0833	0.0540	0.0568	0.0277
$^{87}Sr/^{86}Sr$	0.70723	0.70729	0.70624	0.70905	0.70792	0.70911
Error Sr/Sr	0.001	0.003	0.002	0.002	0.001	0.002
Sm(ppm)	2.43	2.46	2.98	3.25	4.44	4.95
Nd(ppm)	8.43	8.46	9.63	11.64	14.09	18.20
$^{147}Sm/^{144}Nd$	0.1742	0.1762	0.1869	0.1687	0.1908	0.1646
$^{143}Nd/^{144}Nd$	0.512682	0.512680	0.512554	0.512675	0.512721	0.512569
Error Nd/Nd	0.002	0.002	0.002	0.003	0.002	0.003
$\varepsilon Nd_{(0)}$	0.9	0.8	-1.6	0.7	1.6	-1.3
$\varepsilon Nd_{(T)}$	3.0	2.6	0.8	2.3	2.6	1.5
$T_{DM(Ga)}$	1.18	1.32	1.48	1.46	1.62	1.31

excluded from the calculation. If fit indices exceeded the value allowable for 95% confidence in the P-T result, then the most suspected activity (largest e*) was removed and the calculation was re-run (c.f. Powell and Holland, 1994). The results are shown in Table 4.

RESULTS

Petrography

The studied metabasites correspond to metagabbros (gabbro/dolerite sills) and metabasalts. Metagabbros show medium- to coarse-grained textures (Fig. 4A-D) and are mainly composed of albitized plagioclase (45-55vol.%), zoned amphibole (40-50vol.%), and minor chlorite, epidote, and quartz, associated with accessory minerals such as ilmenite, biotite, rutile, magnetite, titanite, and apatite. Plagioclase crystals vary in texture from euhedral to anhedral, with sizes between few micrometers to 3mm, and can host amphibole inclusions up to 50μm. Amphibole grains are subhedral to anhedral, with sizes between 0.2 and 1.5mm, and show green-brown pleochroism in plane-polarized light (Fig. 4A, C). In some samples, large (1-3mm) plagioclase and amphibole crystals are enclosed in a fine-grained matrix of plagioclase and amphibole. Epidote is also a common phase in all samples from both massifs. The metabasites from the Canigó massif show accessory ilmenite grains up to 2mm partially replaced by rutile and titanite (Fig. 5A-B), whereas ilmenite in the Cap de Creus metabasites occurs as skeletal crystals intergrown with silicates and hosting multiple silicate inclusions (biotite, chlorite) (Fig. 5C-D). Apatite (up to 70μm) is also quite common in the Cap de Creus studied samples (Fig. 5E). Chlorite appears in all the studied samples and the mineral association indicates greenschist to lower epidote–amphibolite metamorphic facies.

Metabasalts show a relict flow texture as observed in Figure 4E-G and are mainly composed of amphibole (45-60vol.%) and plagioclase (50-55vol.%), and minor proportion of chlorite and epidote, with accessory ilmenite, titanite, calcite, and quartz. Amphibole grains can host plagioclase (up to 100μm), titanite (up to 240μm), and/or small quartz inclusions (<5μm) (Fig. 5F). Some samples show banded textures with alternating amphibole- and plagioclase-rich bands (Fig. 4G). Mineral grains are subhedral to anhedral with a grain size between a few micrometers and 500μm for plagioclase and amphibole, and up to 100μm for chlorite, epidote, titanite, and ilmenite. Larger crystals (200-500μm) are embedded in a microcrystalline matrix (Fig. 4E-F). Chlorite and epidote are abundant (Fig. 5F-G) and the mineral association indicates greenschist to lower epidote–amphibolite metamorphic facies.

Samples CG-18-02 and CG-18-03 are chlorite-rich schists composed mainly of quartz, plagioclase, and chlorite ± muscovite ± biotite, with accessory subhedral zircon, titanite, apatite, and calcite (Figs. 4H; 5H). The samples show mm-wide mica-rich bands. Zircon grains were separated from CG-18-02 because of its close

TABLE 4. Results of average P-T calculations for the metabasites from the Canigó and Cap de Creus massifs (Eastern Pyrenees). The data includes the corresponding correlations and sigfit value. The sigfit value shows the quality of how well the activities of the selected endmembers match among one another, indicating more accurate and reliable results for the smaller values (Powell and Holland, 1994)

Sample	Massif	Temperature (ºC)	Pressure (kbars)	Cor - SigFit
CC-18-01	Cap de Creus	452 ± 36	6.1 ± 1.6	0.831 – 1.62
CC-18-02	Cap de Creus	482 ± 31	7.7 ± 1.3	0.811 – 1.30
CC-18-03	Cap de Creus	479 ± 19	5.2 ± 0.9	0.885 – 0.85
CG-18-01	Canigó	465 ± 23	6.2 ± 0.9	0.826 – 1.10
CG-18-04	Canigó	452 ± 58	7.2 ± 2.5	0.780 – 2.63

location with the metabasites in order to precise the age of these rocks. Both samples are not included in the mineral chemistry and geochemistry sections.

Mineral chemistry

Representative analyses of the studied minerals in the metabasites are documented in Appendix I. Amphibole is calcic (Ca^B=1.80-1.95apfu), with moderate variation in Si (6.33-7.81apfu) and Mg# (0.35-0.80). Amphibole from samples of the Canigó massif has magnesio-hornblende to actinolite compositions (Fig. 6A), with high Si (7.33-7.81apfu) and Ca (1.80-1.97apfu), and low Al (0.22-0.92apfu) and Na (0.02-0.14apfu), whereas amphibole from samples of the Cap de Creus massif has ferro- to magnesio-tschermakite, ferro- to magnesio-hornblende to actinolite compositions (Fig. 6A), with variable Si (6.33-7.69apfu) and Ca (1.79-1.97apfu), and moderate Al (0.32-2.56apfu) and Na (0.06-0.51apfu).

Plagioclase from metabasites of the Canigó massif corresponds to albite, whereas that from the samples from Cap de Creus massif corresponds to oligoclase-albite and only sample CC-18-01 has plagioclase with andesine composition (Fig. 6B). Chlorite in the samples from the Canigó massif has ripidolite to pycnochlorite compositions (Fig. 6C), with Si content ranging from 5.34 to 5.58apfu and Mg#=0.55-0.63. Chlorite in samples from the Cap de Creus massif corresponds to ripidolite and brunsvigite (Fig. 6C) with Si content ranging from 5.26 to 5.78apfu and Mg#=0.41-0.57. Epidote crystals have low to moderate pistacite content (Xps=Fe^{3+}/[Al-2]+Fe^{3+}] ranging from 0.25 to 0.44 in samples collected in the Canigó massif and from 0.39 to 0.42 in samples collected in the Cap de Creus massif (Fig. 6D).

P-T conditions

Average P-T conditions were determined for samples CG-18-01 and CG-18-04 from the Canigó massif and for samples CC-18-01, CC-18-02, and CC-18-03 from the Cap de Creus massif. The calculated peak conditions used the assemblage Amp + Czo + Pl + Ep + Qtz and the accessory minerals (Ilm, Rt, Mt, and Ttn) were included in the corresponding samples. The obtained results (shown in Table 4 and Figure 7, including the uncertainties) for samples from the Canigó massif are 465±23ºC and 6.2±0.9kbar (CG-18-01) and 452±58ºC and 7.2±2.5kbar (CG-18-04), whereas for samples from the Cap de Creus massif are 452±36ºC and 6.1±1.6kbar (CC-18-01); 482±31ºC and 7.7±1.3kbar (CC-18-02), and 479±19ºC and 5.2±0.9kbar (CC-18-03). These data confirm the greenschist to lower epidote–amphibolite metamorphic facies for the massifs as already suggested by the mineral association (Fig. 7).

Whole-rock geochemistry

Major and minor elements

All the studied metabasites from the Eastern Pyrenees show SiO_2 content between 44.93 and 52.84wt.% (Table 2) and can be classified as sub-alkaline basalts on the Zr/Ti vs. Nb/Y classification diagram of Pearce, 1996 after Winchester and Floyd (1977) (Fig. 8A). Metagabbros and metabasalts have similar compositions and, hence, no differentiation can be made based on their geochemistry (Table 2). The studied metabasites are characterized by Al_2O_3 content ranging between 12.26 and 17.74wt.%, 5.07-11.1wt.% MgO, 9.56-15.26wt.% Fe_2O_3, 7.21-10.65wt.% CaO, 2.19-4.25wt.% Na_2O, moderate content of TiO_2 (up to 2.08wt.%), and relatively low content in Cr (43-416ppm), K_2O (up to 0.32wt.%), and MnO (up to 0.22wt.%), and variable LOI values (0.23-4.22wt.%). The Mg# [Mg/(Mg+Fe^{2+})] is between 0.27 and 0.52, indicating evolved basaltic rocks (Hanson and Langmuir, 1978). The Zr vs. Y discrimination diagram of Ross and Bédard (2009) modified by Barrett and MacLean (1997) shows that all the studied metabasites belong to the transitional magmatic suites, with minor tholeiitic signatures for the Cap de Creus massif samples (Fig. 8B). In the AFM diagram (Irvine and Baragar, 1971), these rocks plot in the center of the tholeiitic field and in the limit tholeiite – calc-alkaline series (Fig. 8C).

Trace elements

Figure 9A shows the Rare Earth Element (REE) contents normalized to chondrite, and Figure 9B illustrates

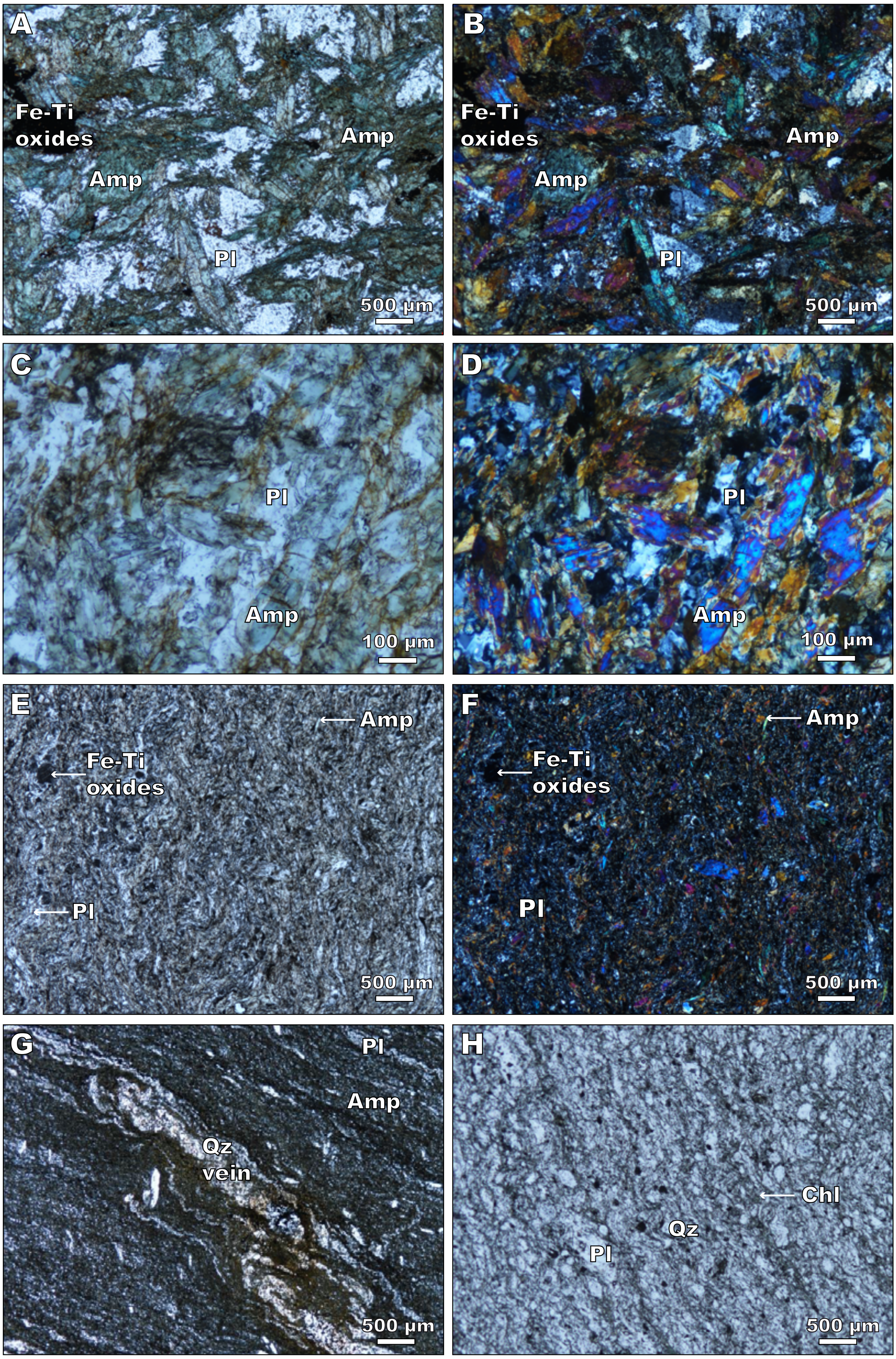

Figure 4. Photomicrographs (plane-polarized and cross-polarized light) of the studied metabasites and chlorite-rich schist showing the different mineral phases. A-D) Metagabbros, E-G) Metabasalts and H) Chlorite-rich schist. A-B) Sample CC-18-02, C-D) Sample CC-18-01, E-F) Sample CG-18-01, G) Sample CC-18-03 and H) Sample CG-18-02. Abbreviations: Amp= amphibole, Chl= chlorite, Pl= plagioclase, Qz= quartz.

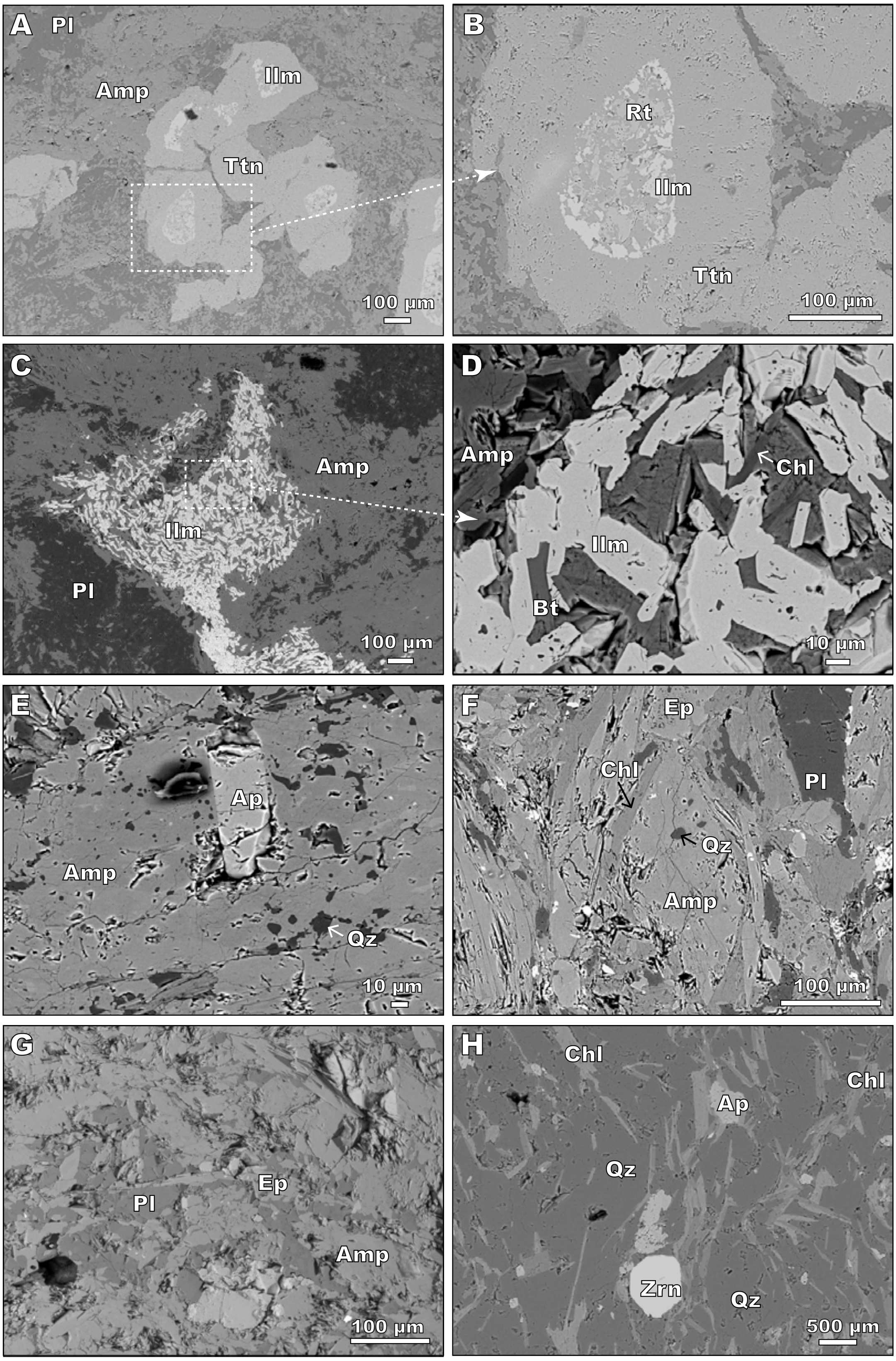

Figure 5. Backscattered electron images of the studied samples showing the different mineral phases. A-B) Metagabbros from the Canigó massif, C-E, F) Metabasalt form the Canigó massif G) Metagabbros from the Cap de Creus massif, and H) Chlorite-rich schist from the Canigó massif. A-B) Sample CG-18-04, C-E) Sample CC-18-02, F) Sample CG-18-01, G) Sample CC-18-01 and H) Sample CG-18-02. Abbreviations: Amp= amphibole, Ap= apatite, Bt= biotite, Chl= chlorite, Ep= epidote, Ilm= ilmenite, Pl= plagioclase, Qz= quartz, Rt= rutile, Ttn= titanite Zrn= zircon.

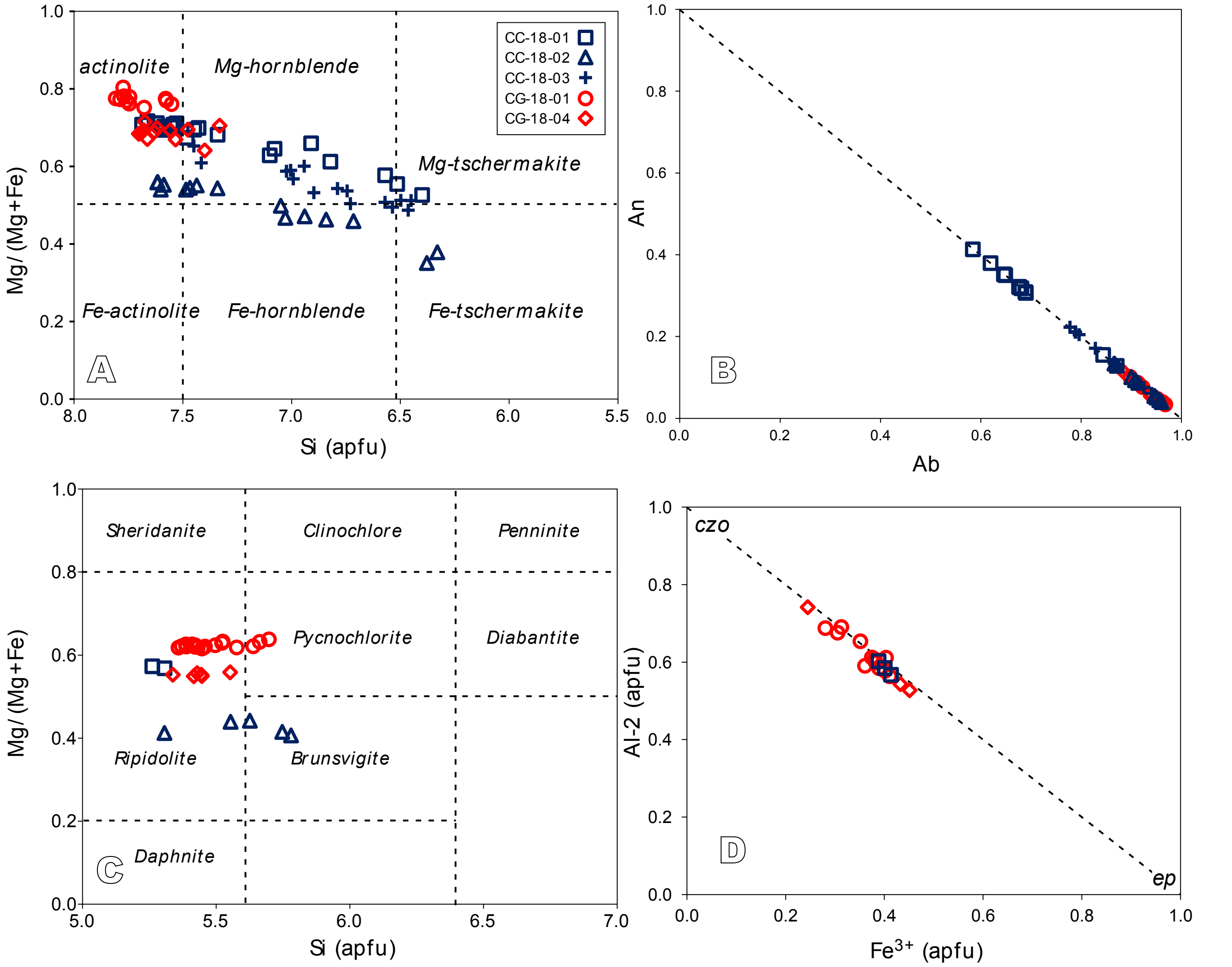

Figure 6. A) Amphibole classification diagram (Leake *et al.*, 1997; Hawthorne *et al.*, 2012). B) Plagioclase composition. C) Chlorite composition in the classification diagram modified from Hey (1954). D) Epidote composition.

the incompatible trace elements normalized to N-MORB for the studied metabasites (normalization values from Sun and McDonough, 1989). All metabasite samples exhibit similar patterns in both REE and spider diagrams, even though samples from the Cap de Creus massif are slightly more enriched in REE (Fig. 9). Total REE concentrations are between 44 and 94ppm (Table 2), values of $(La/Sm)_n/(Gd/Lu)_n$ are between 0.9 and 1.3, and Eu-anomalies are negligible to slightly positive (Eu/Eu*=1.0-1.2). The REE patterns show a negative slope from La to Lu (Fig. 9A), indicating a moderate enrichment in Light Rare Earth Elements (LREE) relative to Heavy Rare Earth Elements (HREE), with an average $(La/Lu)_n$ of 2.7. In the N-MORB-normalized spider diagrams (Fig. 9B), the patterns of the studied metabasites show negative slopes, with marked negative anomalies in Nb [$(Nb/La)_{NMORB}$=0.33-0.78] and positive anomalies in Th [$(Th/La)_{NMORB}$=2.02-5.18]. The obtained patterns are similar to those from other Ediacaran metabasites in the Pyrenees (Padel *et al.*, 2018a), and distinctly different from Pyrenean Ordovician metabasites (*i.e.* see the difference in Nb in Fig. 9B; Navidad *et al.*, 2018).

Sr and Nd isotope geochemistry

Sr and Nd isotopic ratios of the studied metabasites from the Eastern Pyrenees are presented in Table 3. The obtained results are very similar for the metabasites from the Canigó and Cap de Creus massifs. Based on their approximate U-Pb crystallization age of 580Ma (Casas *et al.*, 2015), the initial Sr and Nd isotopic ratios for metabasites were recalculated (formulas by DePaolo and Wasserburg, 1976 and DePaolo, 1981). The initial radiogenic isotope ratios are 0.511932-0.512047 for $^{143}Nd/^{144}Nd$ and 0.705565-0.708882 for $^{87}Sr/^{86}Sr$. They show positive $\varepsilon_{Nd(T)}$ values between 0.82 and 3.05 with T_{DM} model ages of 1.2 to 1.6Ga (Fig. 10). The $\varepsilon_{Nd(T)}$ values are lower than those expected for magmas derived from a depleted mantle source, although

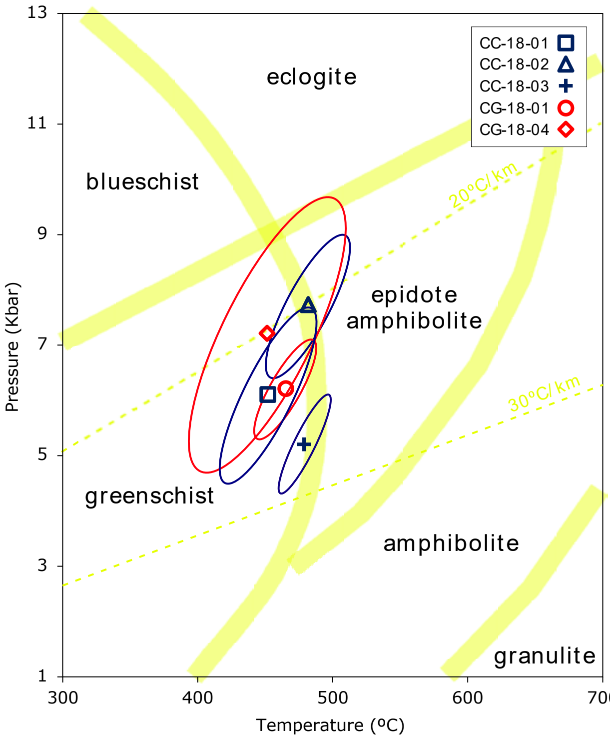

Figure 7. P-T conditions determined by average P-T, including the uncertainty ellipses, calculated following Powell and Holland (1994). The thick lines separate facies fields simplified after Spear (1993).

the positive $\varepsilon_{Nd(T)}$ values preclude a remarkable contribution from an older continental crust (Padel *et al.*, 2018a). In addition, the studied Ediacaran metabasites clearly differ from the Ordovician metabasites from the Eastern Pyrenees (Navidad *et al.*, 2018) that show negative $\varepsilon_{Nd(T)}$ (0.41 to -0.58) and T_{DM} model ages of 1.1-1.3Ga (Fig. 10). Data for the Montemolín metabasites from the Serie Negra Group in Ossa Morena (Rojo-Pérez *et al.*, 2022) have been also included in the diagram, which show a similar range of $\varepsilon_{Nd(T)}$ (from 2.1 to -1.0) but significantly older T_{DM} model ages (1.31-2.11Ga).

U/Pb dating on zircon

Zircon grains were dated in sample CG-18-02 from the Canigó massif, which is a chlorite-rich schist in spatial contact with the metabasites (sample CG-18-01) (Table VI). The analyzed zircon grains range from 50 to 125μm in size, are mostly colorless, euhedral to anhedral in shape, with variable zoning, and show no mineral inclusions. Out of the 81 analyses, 17 of them are ±10% discordant. The Kernel Density Estimate (KDE) plot (Fig. 11) shows one main peak at 632Ma and other, smaller, peaks at 550Ma (limit Paleozoic-Neoproterozoic), 806Ma (Neoproterozoic), 994 Ma (limit Neoproterozoic-Mesoproterozoic), and at 2496Ma (limit Paleoproterozoic-Archean). The zircon grains with Neoproterozoic dates (542-1000Ma) represent

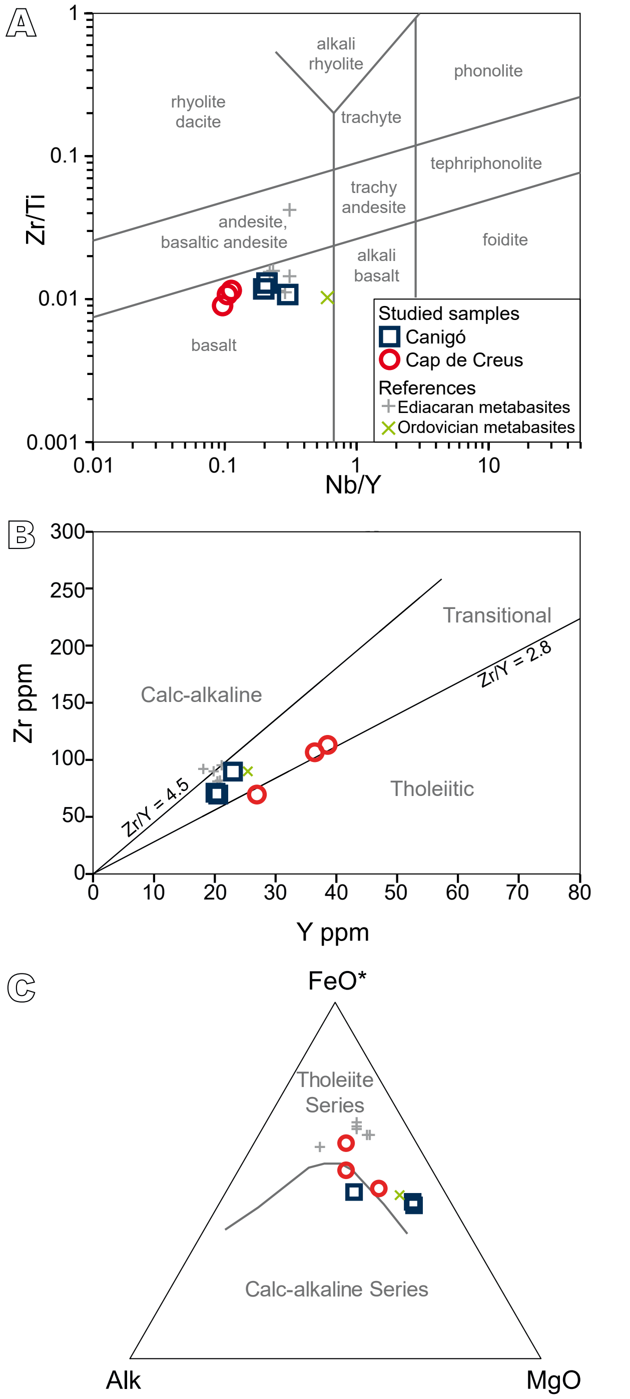

Figure 8. Classification diagrams for the studied metabasites. A) Zr/Ti vs. Nb/Y diagram (Pearce, 1996 after Winchester and Floyd, 1977). B) Zr vs. Y diagram (Ross and Bédard, 2009 modified from Barrett and MacLean, 1997). C) AFM diagram (Irvine and Baragar, 1971). References for metabasites in the Pyrenees are from Navidad *et al.* (2018) for Ordovician metabasites and Padel *et al.* (2018a) for Ediacaran metabasites.

74.7% of the analyses, 3.8% of the analyses have Late Mesoproterozoic ages (1000-1200Ma), 17.7% of the analyses have Paleoproterozoic ages (1600-2500Ma), and only 3.8% of analyses have Archean (>2500Ma) ages. The

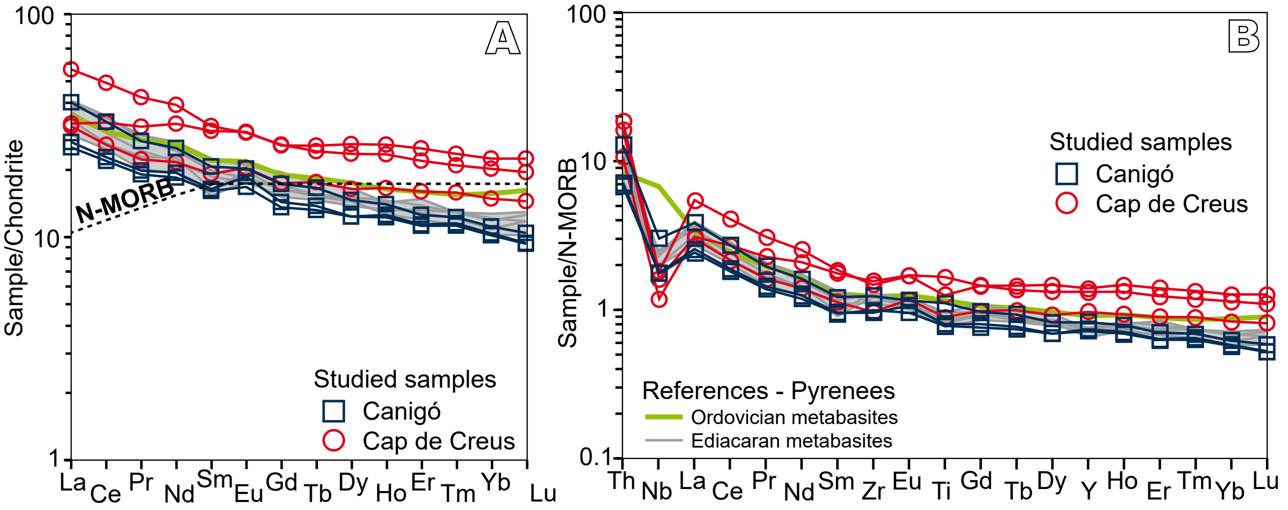

Figure 9. A) Chondrite-normalized REE patterns and B) primitive mantle-normalized patterns for the studied metabasites. Normalizing values from Sun and McDonough (1989). References for metabasites in the Pyrenees are from Navidad *et al.* (2018) for Ordovician metabasites and Padel *et al.* (2018a) for Ediacaran metabasites.

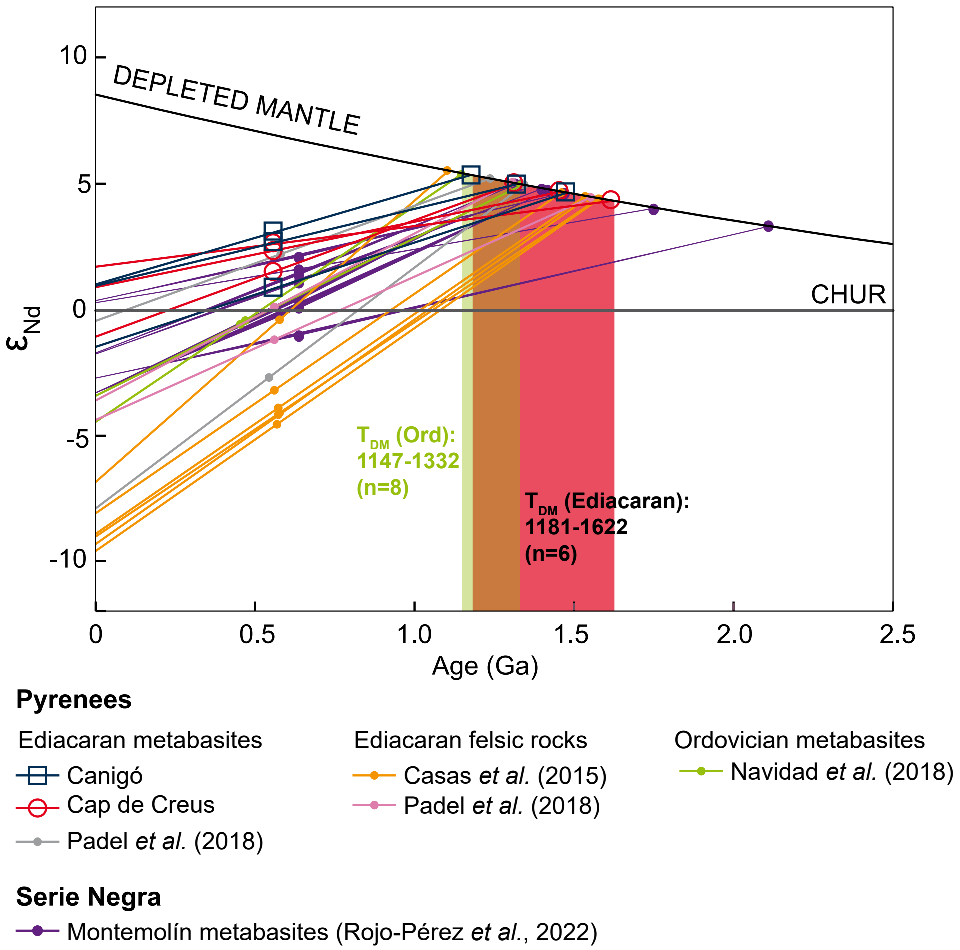

Figure 10. εNd vs. age diagram showing T_{DM} values for the studied metabasites from the Eastern Pyrenees and for other Pyrenean Ediacaran metabasites and felsic rocks (Casas *et al.*, 2015; Padel *et al.*, 2018a), Pyrenean Ordovician metabasites (Navidad *et al.*, 2018), and the Ediacaran Montemolín metabasites from the Serie Negra in the Ossa-Morena Zone (Rojo-Pérez *et al.*, 2022). Depleted mantle evolution is calculated according to DePaolo (1981). CHUR= Chondritic Uniform Reservoir. The range of Nd model ages of selected regions is shown for comparison.

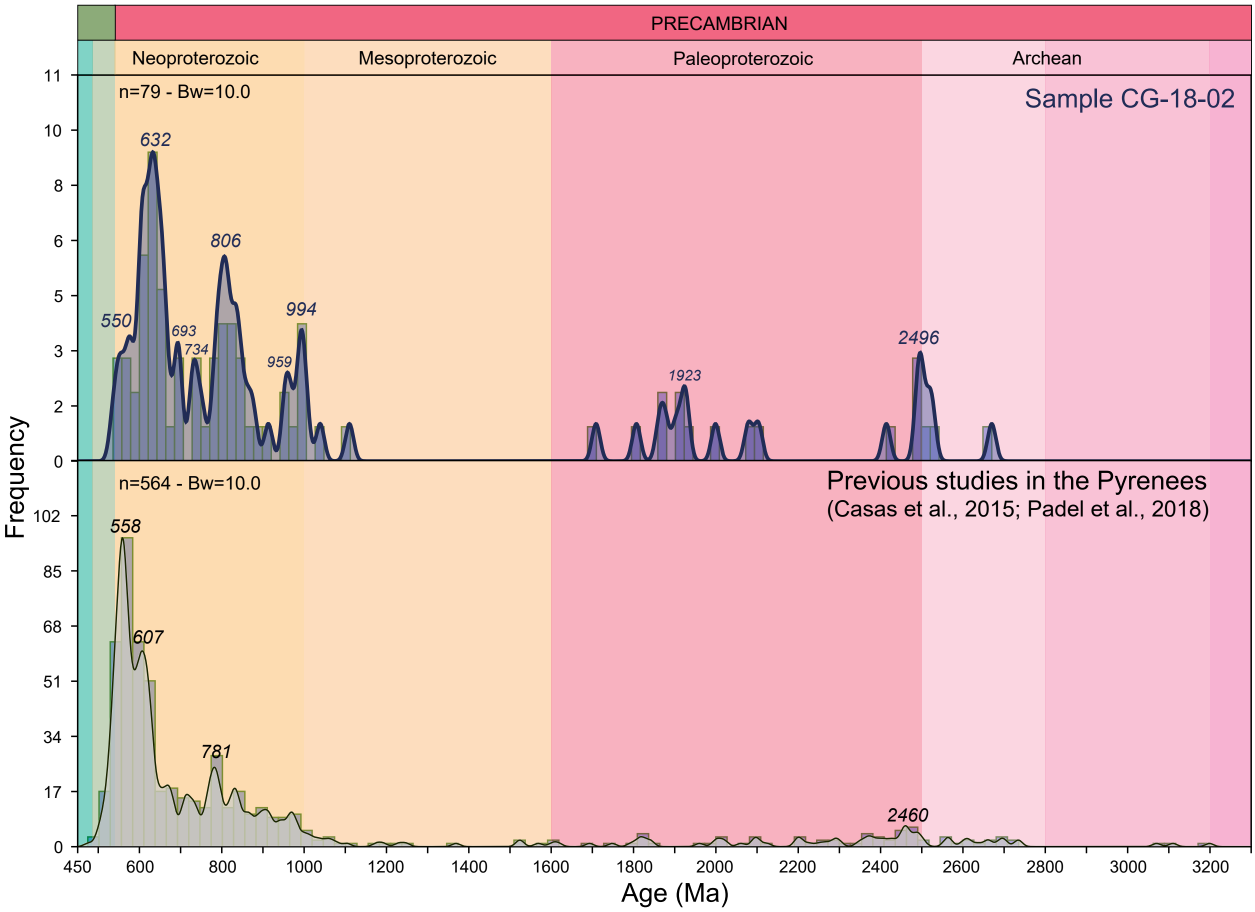

Figure 11. Kernel Density Estimates (KDE) plots, showing the peak ages, for the analyzed sample (CG-18-02) in the top, compared with previous data of Cadomian magmatism in the Pyrenees (Casas *et al.*, 2015; Padel *et al.*, 2018a) at the bottom. Abbreviations: Bw= Band width, n= number of samples. Figure elaborated with the HistogramsApp (Rodriguez-Corcho *et al.*, 2020; Rodriguez-Corcho and action users, 2021).

obtained data shows a broad range of detrital zircon ages, and the distribution is very similar to those observed in previous works (Fig. 11; Padel *et al.*, 2018a). Even though the main peak is at 632Ma, indicating a magmatic event, the smaller peak of 550Ma could represent the maximum depositional age of the metasedimentary chlorite-rich schist.

Previous studies of the Edicaran magmatism in the Pyrenees obtained ages of ca. 565-552Ma (Padel *et al.*, 2018a) for the Canigó massif (Tregurà for these authors), and minimum ages of 575-568Ma (Casas *et al.*, 2015) for the felsic rocks in the Canigó and Cap de Creus massifs. However, the precise age of the Ediacaran mafic magmatism is still an unresolved matter. Geochronological studies from the Ediacaran section of the SW Iberian massif obtained older ages for the metabasites in the Serie Negra, for instance, ages pre 602Ma are assumed for the protolith of the Montemolín metabasites (Rojo-Pérez *et al.*, 2022), and even older ages for the Group 3 amphibolites of Sánchez-Lorda *et al.* (2014), extending the onset of the Cadomian arc mafic magmatism to the latest Cryogenian – earliest Ediacaran (645±17Ma; Sánchez-Lorda *et al.*, 2016).

DISCUSSION

The geochemical characteristics of the studied metabasites from the Canigó and Cap de Creus massifs indicate that these correspond to rocks with basaltic composition with transitional signatures between tholeiite and calc-alkaline (Fig. 8) with affinities of volcanic arc basalts (Fig. 12A-B). The chondrite-normalized REE patterns of these metabasites (Fig. 9) are similar to those from normal Island Arc Tholeiites (IAT; see normal IAT basalts from Escuder-Viruete *et al.*, 2006), whereas they clearly differ from typical patterns for N-MORB and OIB basalts (Sun and McDonough, 1989). The N-MORB normalized multielement patterns of the studied rocks are also similar to those from normal IAT basalts (Escuder-Viruete *et al.*, 2006; Torró *et al.*, 2017 and references therein), contrasting with the patterns for rocks formed

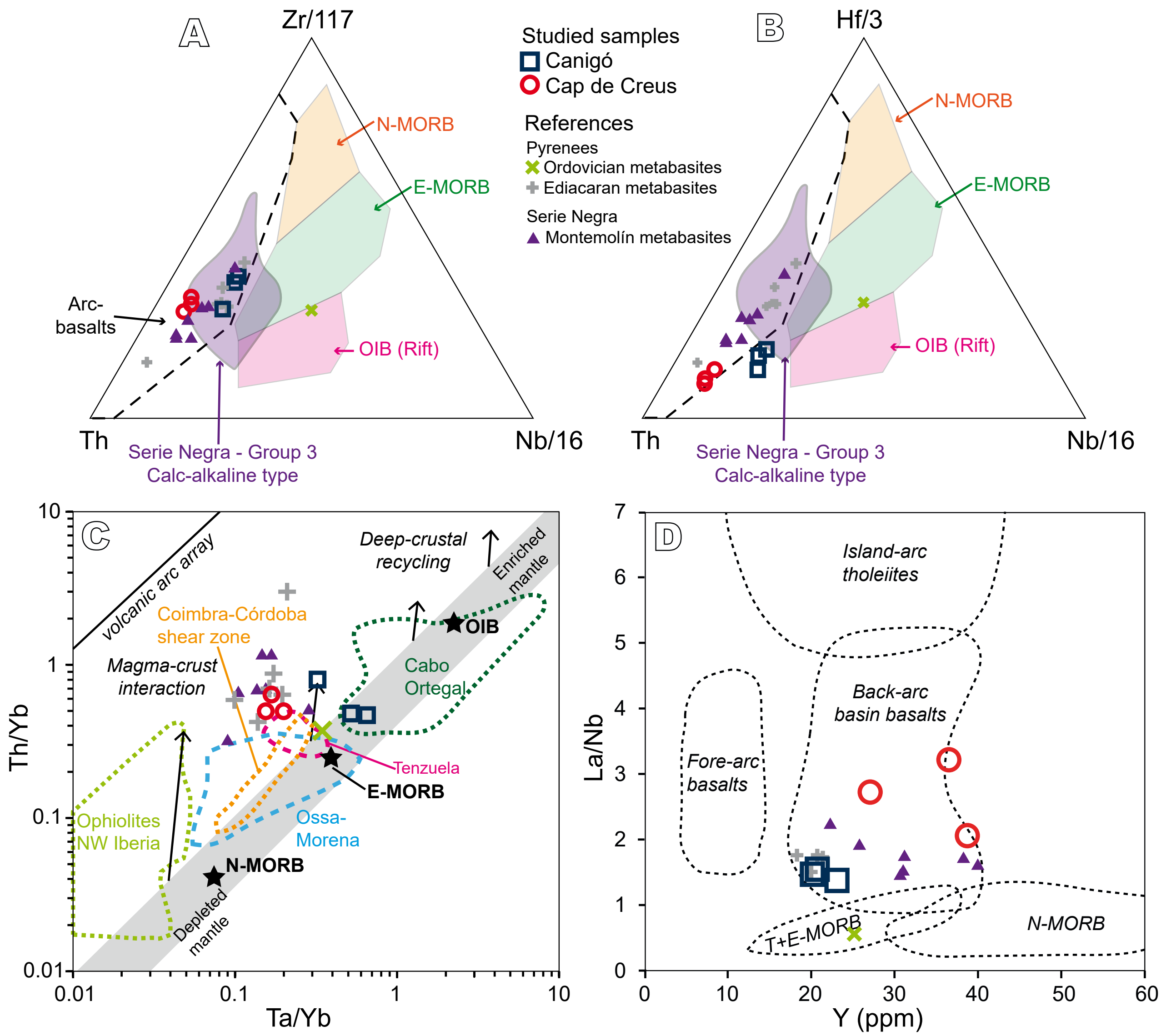

Figure 12. Tectonic setting of the studied Ediacaran metabasites. A-B) Th-Zr/117-Nb/16 and Th-Hf/3-Nb/16 ternary plots from Wood (1980). Serie Negra metabasites data from Sánchez-Lorda *et al.* (2014). C) Th/Yb vs. Ta/Yb. Diagram from Pearce (2008), fields compiled by Villaseca *et al.* (2015). D) La/Nb vs. Y (ppm). Fields from Ouabid *et al.* (2020) after Floyd *et al.* (1991). References for metabasites in the Pyrenees are from Navidad *et al.* (2018) for Ordovician metabasites and Padel *et al.* (2018a) for Ediacaran metabasites, and references for the Ediacaran Montemolín metabasites from the Serie Negra is from Rojo-Pérez *et al.* (2022).

during the initial stages of oceanic subduction (*e.g.* FAB, boninites; see Reagan *et al.*, 2010). Trace elements also show relatively high Th/Yb ratios (Th/Yb=0.5-0.8) possibly indicating influence by a subduction-enriched mantle (Fig. 12C) (Pearce, 2014; Shervais, 2022 and references therein), whereas the low TiO_2/Yb (0.4-0.7) and variable Nb/Yb (0.9-3.7) ratios suggest a heterogeneous enriched shallow mantle source (characteristic of the spinel lherzolite stability field) without any contribution of OIB components (Pearce, 2014). In addition, trace element variations are akin to arc lavas generated in slab-distal back-arc basins (Fig. 12D) and clearly different from those of magmas formed during initial stages of oceanic subduction (*e.g.* FAB-boninites-Low-Ti (LOTI)- Island Arc Tholeiites (IAT) in the IBM in the Izu-Bonin-Mariana arc; Ishizuka *et al.*, 2011; Reagan *et al.*, 2010; Torró *et al.*, 2017). Studied metabasites systematically have Ti/V>20, consistent with lavas from Andean-type convergent continental margins (Shervais *et al.*, 2022, fig. 9). As stated above, the obtained compositions are similar to other metabasites with an Ordovician or a putative Ediacaran age previously described in the Pyrenean area (Figs. 8; 9; 12; Navidad *et al.*, 2018; Padel *et al.*, 2018a). However, all the studied metabasites show a pronounced negative Nb anomaly in the N-MORB normalized spider diagrams (Fig. 9), whereas the Ordovician metabasites from the Canigó massif (one sample from Navidad *et al.*, 2018) show a positive anomaly in Nb. This positive anomaly indicates a contaminated E-MORB source for the Ordovician rocks (Navidad *et al.*, 2018). These marked differences are also observed in the isotopic compositions: the studied Ediacaran metabasites from the Canigó and Cap de Creus massifs show positive $\varepsilon_{Nd(T)}$ values (0.82-3.05), which excludes a remarkable contribution from an older continental crust (Fig. 10), whereas the Ordovician ones show negative ε_{Nd} (Navidad *et al.*, 2018).

The trace elements of the studied Ediacaran metabasites from the Eastern Pyrenees are also similar to those from the Group 3 amphibolites from the Ediacaran Serie Negra Group of the Ossa-Morena Zone (SW Iberia) (Sánchez-Lorda *et al.*, 2014) and to the metabasites hosted within the Montemolín Formation from the Serie Negra (Rojo-Pérez *et al.*, 2022). Both the Group 3 metabasites and the Montemolín metabasites from the Serie Negra are classified as basalts and their trace elements indicate volcanic arc signatures (Fig. 12A-B) related to an enriched mantle source modified by subducted slab components (Rojo-Pérez *et al.*, 2022). In addition, the Group 3 amphibolites are spatially associated with metabasites showing N-MORB signatures, which have been interpreted as FAB, and metabasites showing E-MORB signatures (Group 1 and 2 respectively in Sánchez-Lorda *et al.*, 2014). Based on these associations, Sánchez-Lorda *et al.* (2014) interpreted a N-dipping (in present-day geography) subduction of oceanic lithosphere beneath Gondwana during the late Ediacaran. The metabasites from the Serie Negra (Sánchez-Lorda *et al.*, 2014, 2016) with different signatures allow tracing this event from subduction-initiation (formation of FAB) to the development of a volcanic arc edifice on the thinned Gondwana margin during the latest Ediacaran to Terreneuvian. These authors also found E-MORB metabasites that interpreted as related to recycled oceanic crust, to a metasomatically enriched lithospheric mantle, or to recycling of alkaline basalts.

When comparing the trace elements content of the metabasites with those of the felsic rocks from the Eastern Pyrenees (Casas *et al.*, 2015; Padel *et al.*, 2018a), the higher silica rocks are more enriched in REE and trace elements. However, the patterns show similar trends and slopes, thus, an origin of these felsic rocks related to magmatic fractionation of mafic melts cannot be completely ruled out. Regarding the isotopic analyses, the T_{DM} model ages obtained for the mafic (1.2-1.6Ga) and the felsic (1.1-1.5Ga; Casas *et al.*, 2015; Padel *et al.*, 2018a) rocks are within the same range (Fig. 10), even though the mafic samples indicate slightly older model ages. Casas *et al.* (2015) interpreted that the Pyrenean Ediacaran felsic magmatism took place in a back-arc environment and that it represents evidence of a long-lived subduction-related magmatic arc. Padel *et al.* (2018a) linked the Ediacaran mafic rocks in the Eastern Pyrenees to an extensional event and interpreted that these extensional conditions predated the Cadomian magmatism that formed the felsic rocks. In addition, Padel *et al.* (2018a) related this felsic magmatism to the final stages of the volcanic arc related to the SW-NE trending *peri*-Gondwana subduction that migrated from the Moroccan (Anti-Atlas) to the Ossa-Morena and Cantabrian zones.

The distribution of ages obtained for the studied chlorite-rich schist in close contact with the metabasites from the Eastern Pyrenees provides evidence of a Cadomian magmatic activity in the area. The younger peak in the obtained density distribution curve (Fig. 11) has an age of 550Ma, and probably represents the maximum depositional age for the metasedimentary chlorite-rich schist, but the stronger peak is at 632Ma and probably indicates magmatism around this age during the Cadomian. Hence, Cadomian magmatic activity could have started earlier than suggested in previous works (545Ma in Mezger and Gerdes, 2016, or 543Ma and 533Ma in Padel *et al.*, 2018a). Actually, similar zircon age peaks were obtained for the felsic metavolcanics of the Canigó massif (600-640Ma, Castiñeiras *et al.*, 2008; Padel *et al.*, 2018a), for the Aston massif (ca. 608Ma, Gnioure paragneiss, Mezger and Gerdes, 2016), which indicates a long-lasting stepwise Cadomian magmatic activity in the Pyrenees, ranging from 630 to 530Ma approximately. In fact, the very similar (based on the geochemistry and $\varepsilon_{Nd(T)}$ values; Figs. 10; 12) metabasites within the Montemolín Fm. in the Serie Negra (Rojo-Pérez *et al.*, 2022) have been interpreted as formed from a >602Ma protolith, which could have similar ages to the main magmatic peak that is observed in our study for the Pyrenean metabasites. Besides, other works in the Serie Negra suggest that the onset of the Cadomian arc magmatism could be further extended to the earliest Ediacaran (Sánchez-Lorda *et al.*, 2016). Therefore, the main peak at 632Ma obtained for the detritic rock (chlorite-rich schist) related to the direct dismantlement of the metabasites may indicate a major magmatic event during the Cadomian–Pan-African orogenies.

The tectonic setting depicted here may reflect the later stages of the Cadomian orogeny in this area, far from the main sutures, in which bimodal felsic and mafic magmatism are coeval. The Pyrenean margin would embrace the northwest margin of Gondwana during Ediacaran times (Fig. 13), extending from the Ossa-Morena Zone to the southwest (Rubio-Ordóñez *et al.*, 2015; Rojo-Pérez *et al.*, 2019, 2021; Sánchez-Lorda *et al.*, 2014) to the core of the Alpine-Himalayan orogenic system to the northeast through the Turkish massifs as far as the Iranian and Caucasus Mountains (Abbo *et al.*, 2015, 2020; Bendokht *et al.*, 2021; Fiannacca *et al.*, 2013; Micheletti *et al.*, 2007; Moghadam *et al.*, 2015, 2017; Williams *et al.*, 2012; Yilmaz Şahin *et al.*, 2013).

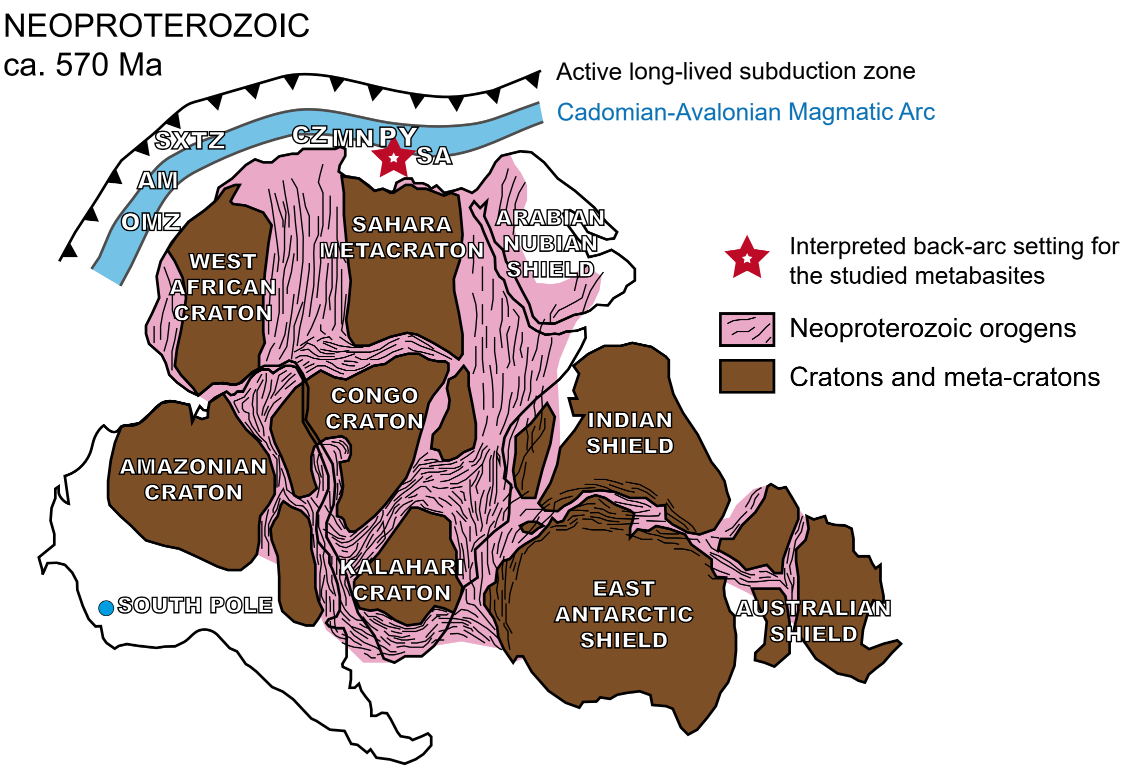

Figure 13. Paleogeographic reconstruction at c. 570Ma showing the interpreted paleo-position for the studied mafic magmatism in the Eastern Pyrenees. Abbreviations: OMZ= Ossa-Morena Zone, AM= Armorican massif, SXTZ= Saxo-Thuringian Zone, CZ= Cantabrian Zone, MN= Montagne Noire, PY= Pyrenees and SA= Sardinia. Figure modified from Rojo-Pérez *et al.* (2021), who based the Gondwana paleogeography on von Raumer and Stampfli (2008), Meert and Lieberman (2008), and Díez Fernández *et al.* (2010). The position of the different units along the northern Gondwana margin is after Casas and Murphy (2018) and Rojo-Pérez *et al.* (2021).

The peak P-T conditions of 452-482ºC and 5.2-7.7kbar for the studied metabasites from the Eastern Pyrenees suggest that the rocks reached depths down to approximately 16 to 23km during prograde (burial + heating) metamorphism (Fig. 7). These data give an apparent geothermal gradient of 20-28ºC/km, typical of intermediate P/T metamorphic field gradients (*i.e.* Barrovian type; Fig. 14) generally considered collision-related (*e.g.* Brown, 2007, 2009). These conditions are similar to the previous P-T data for the Variscan metamorphism recorded in the Canigó massif (Fig. 14; Ayora *et al.*, 1993), where P-T conditions of 4.6-6kbar and 450-530ºC were calculated for an early metamorphic Barrovian medium-P metamorphism coeval with the main deformation phase, as also suggested in other areas of the Eastern Pyrenees (Druguet, 2001, fig. 9). This episode of Barrovian metamorphism preceded the low-P/high-T metamorphism characteristic of the Variscan orogeny in the Pyrenees (Ribeiro *et al.*, 2019 and references therein) with maximum P-T conditions around 5-8kbar and 650-840ºC (Aguilar *et al.*, 2015, 2016; Ribeiro *et al.*, 2019) for the sillimanite K-feldspar zone and migmatites. Migmatites from the Eastern Pyrenees were dated to occur in the interval 320-315Ma (Aguilar *et al.*, 2014), thus indicating a Variscan age for the above-mentioned low-P/high-T metamorphism. Even though the previous medium-P metamorphism has been traditionally interpreted as related to the Variscan orogeny it has not been dated, thus a pre-Variscan (Cadomian?) age cannot be completely ruled out.

CONCLUDING REMARKS

The geochemical characteristics, particularly the trace elements, of the studied metabasites from the Eastern Pyrenees (Canigó and Cap de Creus massifs) indicate that these correspond to transitional tholeiite–calc-alkaline basalts with volcanic arc affinities influenced by a subduction-enriched mantle. The studied Pyrenean Ediacaran metabasites are similar to the previous described putative Ediacaran metabasites in the Eastern Pyrenees and to the Group 3 amphibolites and Montemolín metabasites of the Serie Negra Group (Ossa- Morena Zone, SW Iberia), but are clearly different from the Pyrenean Ordovician metabasites. Hence, we argue that the Cadomian metabasites from the Eastern Pyrenees were probably formed during back-arc extension or during the formation of an intra-arc basin in the continental margin of Gondwana. The

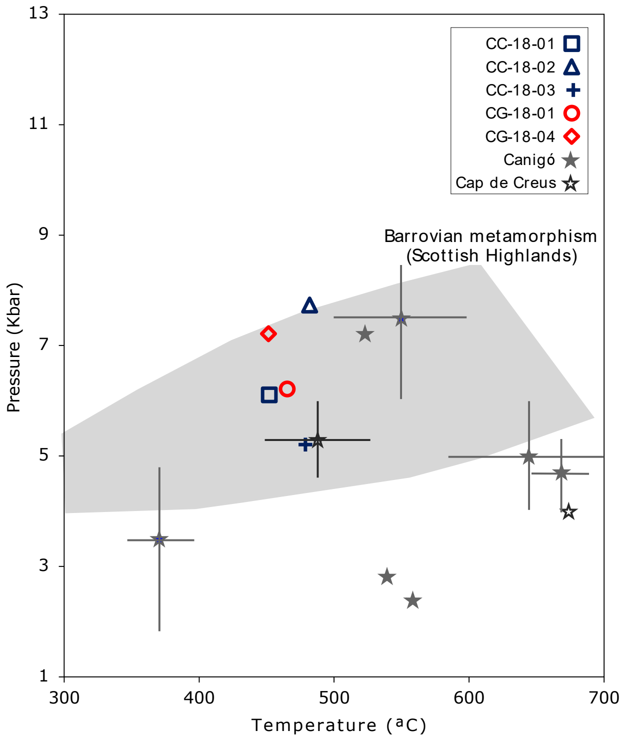

Figure 14. Comparison of average P-T peak conditions in this work with previous published data from the Canigó and Cap de Creus massifs (revision after Ribeiro *et al.*, 2019). The Barrovian metamorphism field is after Spear (1993).

distribution of ages observed in the zircon grains obtained from the chlorite-rich schist in close contact with the metabasites suggests a long-lasting stepwise Cadomian magmatic activity in the Pyrenees, ranging from 630 to 530Ma approximately. Average P-T determinations yield peak conditions of 452-482ºC and 5.2-7.7kbar (depths of 16-23km), with an apparent geothermal gradient of 20-28ºC/km. These conditions are typical of intermediate P/T metamorphic field gradients (*i.e.* Barrovian type) generally related to collision. This metamorphism could have taken place during the Variscan orogeny, even though a pre-Variscan age cannot be ruled out.

ACKNOWLEDGMENTS

This research was financially supported by the Spanish Projects CGL2017-87631-P and PGC2018-093903-B-C22, Ministerio de Ciencia, Innovación y Universidades/Agencia Estatal de Investigación/Fondo Europeo de Desarrollo Regional, Unión Europea. Additional funding was provided by a Margarita Salas grant to NPS by the Universitat de Barcelona with funds from the Ministerio de Universidades/NextGenerationEU/PRTR/Plan de recuperación, transformación y resiliencia. We are deeply indebted to María José Aguilar Pérez for sample preparation and processing. Reviewers Antonio Castro and M. Francisco Pereira, and editor Martim Chichorro are deeply acknowledged for their constructive criticism and their very useful comments, which have helped to greatly improve the quality of the present manuscript.

REFERENCES

Abbo, A., Avigad, D., Gerdes, A., Güng, T., 2015. Cadomian basement and Paleozoic to Triassic siliciclastics of the Taurides (Karacahisar dome, south-central Turkey): Paleogeographic constraints from U–Pb–Hf in zircons. Lithos, 227, 122-139. DOI: http://dx.doi.org/10.1016/j.lithos.2015.03.023

Abbo, A., Avigad, D., Gerdes, A., Morag, N., Vainer, S., 2020. Cadomian (ca. 550 Ma) magmatic and thermal imprint on the North Arabian-Nubian Shield (south and central Israel): New age and isotopic constraints. Precambrian Research, 346, 105804. DOI: https://doi.org/10.1016/j.precamres.2020.105804

Aguilar, C., Liesa, M., Castiñeiras, P., Navidad, M., 2014. Late-Variscan metamorphic and magmatic evolution in the eastern Pyrenees revealed by U-Pb age zircon dating. Journal of Geological Society of London, 171, 181-192. DOI: http://dx.doi.org/10.1144/jgs2012-086

Aguilar, C., Liesa, M., Štípská, P., Schulmann, K., Muñoz, J.A., Casas, J.M., 2015. P–T–t–d evolution of orogenic middle crust of the Roc de Frausa Massif (Eastern Pyrenees): A result of horizontal crustal flow and Carboniferous doming? Journal of Metamorphic Geology, 33(3), 273-294. DOI: https://doi.org/10.1111/jmg.12120

Aguilar, C., Liesa, M., Reche, J., Powell, R., 2016. Fluid-fluxed melting and melt loss in a syntectonic contact metamorphic aureole from the Variscan eastern Pyrenees. Journal of Metamorphic Geology, 34(4), 379-400. DOI: https://doi.org/10.1111/jmg.12187

Aiglsperger, T., Proenza, J.A., Zaccarini, F., Lewis, J.F., Garuti, G., Labrador, M., Longo, F., 2015. Platinum group minerals (PGM) in the Falcondo Ni-laterite deposit, Loma Caribe peridotite (Dominican Republic). Mineralium Deposita, 50, 105-123. DOI: https://doi.org/10.1007/s00126-014-0520-9

Álvaro, J.J., Casas, J.M., Clausen, S., Padel, M., Sánchez-García, T., 2018. Cadomian cycle in the Pyrenees. In: Quesada, C., Oliveira, J.T. (eds.). The Geology of Iberia: a Geodynamic Approach. Regional Geology Reviews series. Heidelberg, Springer, 566pp.

Arenas, R., Fernández-Suárez, J., Montero, P., Díez Fernández, R., Andonaegui, P., Sánchez Martínez, S., Albert, R., Fuenlabrada, J.M., Matas, J., Martín Parra, L.M., Rubio Pascual, F.J., Jiménez-Díaz, A., Pereira, M.F., 2018. The Calzadilla Ophiolite (SW Iberia) and the Ediacaran fore-arc evolution of the African margin of Gondwana. Gondwana Research, 58, 71-86. DOI: https://doi.org/10.1016/j.gr.2018.01.015

Ayora, C., Casas, J.M., 1986. Strabound As-Au mineralization in pre-Caradocian rocks form the Vall de Ribes, Eastern Pyrenees, Spain. Mineralium Deposita, 21, 278-287.

Ayora, C., Liesa, M., Delgado, J., 1993. Low-thermal gradient Hercynian metamorphism in the eastern Pyrenees. Journal of Metamorphic Geology, 11, 49-58. DOI: https://doi.org/10.1111/j.1525-1314.1993.tb00130.x

Barrett, T.J., MacLean, W.H., 1997. Volcanic sequences, lithogeochemistry, and hydrothermal alteration in some bimodal volcanic-associated massive sulfide systems. In: Barrie, C.T., Hannington, M.D. (eds.). Volcanic associated massive sulfide deposits: Processes and examples in modern and ancient settings. Reviews in economic geology, 8, 101-131. DOI: https://doi.org/10.5382/Rev.08.05

Bendokht, M., Shabanian, N., Davoudian, A.R., Dong, Y., Cottle, J.M., Johnson, T.A., 2021. Geochronology and geochemistry of Cadomian basement orthogneisses from the Tutak metamorphic Complex, Sanandaj-Sirjan Zone, Iran. Precambrian Research, 362, 106288. DOI: https://doi.org/10.1016/j.precamres.2021.106288

Brown, M., 2007. Metamorphic conditions in orogenic belts: A record of secular change. International Geology Review, 49, 193-234. DOI: https://doi.org/10.2747/0020-6814.49.3.193

Brown, M., 2009. Metamorphic patterns in orogenic systems and the geological record. London, The Geological Society, 318 (Special Publication), 37-74. DOI: https://doi.org/10.1144/SP318.2

Carreras, J., Ramírez, J., 1984. The geological significance of the Port de la Selva Gneisses (Eastern Pyrenees, Spain). International Geoscience Programme Newsletter, 6, 27-31.

Carreras, J., Casas, J.M., 1987. On folding and shear zone development: a mesoscale structural study on the transition between two different tectonic styles. Tectonophysics, 135, 87-98. DOI: https://doi.org/10.1016/0040-1951(87)90154-5

Carreras, J., Capellà, I., 1994. Tectonic levels in the Palaeozoic basement of the Pyrenees: a review and a new interpretation. Journal of Structural Geology, 16, 1509-1524.

Carreras, J., Debat, P. (coord), Alonso, J.L., Andrews, J.R., Autran, A., Barnolas, A., Bessière, G., Besson, M., Bodin, J., Casas, J.M., Cirés, J., Colwill, J., Delvolvé, J.J., Demange, M., Duran, H., Echtler, H., Fonteilles, M., Garcia-Sansegundo, J., Gisbert, J., Guérangé, B., Guérangé-Lozes, J., Guitard, G., Julivert, M., Lamourouz, C., Laumonier, B., Ledru, P., Liesa, M, Llac, F., Losantos, M., Majesté-Menjoulas, C., Mercier, A., Muñoz, J.A., Palau, J., Pequera, N., Poblet, M., Pouget, P., Richard, Ph., Rios, L.M., Roux, L., Schulze, M., Soldevila, J., Soula, J.C., Van den Eeckhout, B., *et al.*, 1996. Tectonique hercynienne. In: Barnolas, A., Chiron, J.C. *et al.* (eds.). Synthèse Géologique et Géophysique des Pyrénées, tome 1 – Cycle Hercynien . BRGM-ITGE, 585-677.

Carreras, J., 2001. Zooming on Northern Cap de Creus shear zones. Journal of Structural Geology, 23, 1457-1486.

Carreras, J., Druguet, E., 2014. Framing the tectonic regime of the NE Iberian Variscan segment. In: Schulmann, K., Martínez Catalán, J.R., Lardeaux, J.M., Janousek, V., Oggiano, G. (eds.). The Variscan Orogeny: Extent, Timescale and the Formation of the European Crust. London, The Geological Society, 405 (Special Publications), 249-264.

Casas, J.M., Martí, J., Ayora, C., 1986. Importance du volcanisme dans la composition lithostratigraphique du Paléozoïque inférieur des Pyrénées catalanes. Comptes Rendus de l'Académie des Sciences, 302, 1193-1198.

Casas, J.M., Castiñeiras, P., Navidad, M., Liesa, M., Carreras, J., 2010. New insights into the Late Ordovician magmatism in the Eastern Pyrenees: U–Pb SHRIMP zircon data from the Canigó massif. Gondwana Research, 17, 317-324. DOI: https://doi.org/10.1016/j.gr.2009.10.006

Casas, J.M., Palacios T., 2012. First biostratigraphical constraints on the pre–Upper Ordovician sequences of the Pyrenees based on organic-walled microfossils. Comptes Rendus Géoscience, 344, 50-56. DOI: https://doi.org/10.1016/j.crte.2011.12.003

Casas, J.M., Navidad, M., Castiñeiras, P., Liesa, M., Aguilar, C., Carreras, J., Hofmann, M., Gärtner, A., Linnemann, U., 2015. The Late Neoproterozoic magmatism in the Ediacaran series of the Eastern Pyrenees: new ages and isotope geochemistry. International Journal of Earth Sciences, 104, 909-925. DOI: https://doi.org/10.1007/S00531-014-1127-1

Casas, J.M., Murphy, J.B., 2018. Unfolding the arc: The use of pre-orogenic constraints to assess the evolution of the Variscan belt in Western Europe. Tectonophysics, 736, 47-61. DOI: https://doi.org/10.1016/J.TECTO.2018.04.012

Castiñeiras, P., Navidad, M., Liesa, M., Carreras, J., Casas, J.M., 2008. U–Pb zircon ages (SHRIMP) for Cadomian and Early Ordovician magmatism in the Eastern Pyrenees: New insights into the pre-Variscan evolution of the northern Gondwana margin. Tectonophysics, 461, 228-239. DOI: https://doi.org/10.1016/J.TECTO.2008.04.005

Castro, A., Corretgé, L.G., Martínez, F.J., Pascual, E., Lago, M., Arranz, E., Galé, C., Fernández, C., Donaire, T., López, S., 2002. Palaeozoic Magmatism. In: Gibbons, W., Moreno, T. (eds.). The Geology of Spain. London, The Geological Society, 118-153. DOI: https://doi.org/10.1144/GOSPP.8

Cavet, P. 1957. Le Paléozoïque de la zone axiale des Pyrénées orientales françaises entre le Roussillon et l'Andorre. Bulletin du Service de la Carte géologique de France, 55, 303-518.

Cocherie, A., Baudin, Th., Autran, A., Guerrot, C., Fanning, C.M, Laumonier, B., 2005. U-Pb zircon (ID-TIMS and SHRIMP) evidence for the early Ordovician intrusion of metagranites in the late Proterozoic Canaveilles Group of the Pyrenees and the Montagne Noire (France). Bulletin de la Société Géologique de France, 176, 269-282. DOI: https://doi.org/10.2113/176.3.269

Díez Fernández, R., Martínez Catalán, J.R., Gerdes, A., Abati, J., Arenas, R., Fernández-Suárez, J., 2010. U–Pb ages of detrital zircons from the Basal allochthonous units of NW Iberia: Provenance and paleoposition on the northern margin of Gondwana during the Neoproterozoic and Paleozoic. Gondwana Research, 18(2-3), 385-399. DOI: https://doi.org/10.1016/J.GR.2009.12.006

Druguet, E., 2001. Development of high thermal gradients by coeval transpression and magmatism during the Variscan orogeny: insights from the Cap de Creus (Eastern Pyrenees).

Tectonophysics, 332, 275-293. DOI: https://doi.org/10.1016/S0040-1951(00)00261-4

Escuder-Viruete, J., Díaz de Neira, A., Hernáiz Huerta, P.P., Monthel, J., Senz, J.G., Joubert, M., Lopera, E., Ullrich, T., Friedman, R., Mortensen, J., Pérez-Estaún, A., 2006. Magmatic relationships and ages of Caribbean Island arc tholeiites, boninites and related felsic rocks, Dominican Republic. Lithos, 90(3-4), 161-186. DOI: https://doi.org/10.1016/J.LITHOS.2006.02.001

Fiannacca, P., Williams, I.S., Cirrincione, R., Pezzino, A., 2013. The augen gneisses of the Peloritani Mountains (NE Sicily): Granitoid magma production during rapid evolution of the northern Gondwana margin at the end of the Precambrian. Gondwana Research, 23(2), 782-796. DOI: https://doi.org/10.1016/J.GR.2012.05.019

Floyd, P.A., Kelling, G., Gökçen, S.L., Gökçen, N., 1991. Geochemistry and tectonic environment of basaltic rocks from the Misis ophiolitic mélange, south Turkey. Chemical Geology, 89, 263-280. DOI: https://doi.org/10.1016/0009-2541(91)90020-R

Gibson, R.L., 1989. The relationship between deformation and metamorphism in the Canigou massif, Pyrenees: a case study. Geologie en Mijnbouw, 68(3), 345-356.

Gibson, R.L., 1992. Sequential, syndeformational porphyroblast growth during Hercynian low-pressure/high-temperature metamorphism in the Canigou massif. Pyrenees Journal of Metamorphic Geology, 10(5), 637-650. DOI: https://doi.org/10.1111/j.1525-1314.1992.tb00112.x

Gibson, R.L., Bickle, M.J., 1994. Thermobarometric constraints on the conditions of metamorphism in the Canigou massif, Pyrenees: implications for Hercynian geothermal gradients. Journal of the Geological Society, 151, 987-997. DOI: https://doi.org/10.1144/gsjgs.151.6.0987

Govindaraju, K., 1994. 1994 compilation of working values and sample descriptions for 383 geostandards. Geostandards Newsletters, 18, 1-158. DOI: https://doi.org/10.1046/J.1365-2494.1998.53202081.X-I1

Govindaraju, K., Potts, P.J., Webb, P.C., Watson, J.S., 1994. 1994 Report on Whin Sill Dolerite WS-E from England and Pitscurrie Micrograbbro PM-S from Scotland: assessment by one hundred and four international laboratories. Geostandards Newsletters, 18, 211-300. DOI: https://doi.org/10.1111/J.1751-908X.1994.TB00520.X

Guitard, G., Laffitte, F., 1956. Sur l'importance et la nature des manifestations volcaniques dans le Paléozoïque des Pyrénées Orientales. Comptes Rendus de l'Académie des Sciences, 242, 2749-2752.

Guitard, G., 1965. Associations minerales, subfacies et types de metamorphisme dans les micaschistes et les gneiss pelitiques du massif du Canigou (Pyrenees-Orientales). Bulletin de La Société Géologique de France, S7-VII(3), 356-382. DOI: https://doi.org/10.2113/GSSGFBULL.S7-VII.3.356

Guitard, G., 1970. Le métamorphisme hercynien mésozonal et les gneiss œillés du massif du Canigou (Pyrénées orientales). Mémoires du Bureau de Recherches Géologiques et Minières, 63, 1-353.

Guitard, G., Vielzeuf, D., Martinez, F., Alias, G., Autran, A., Besson, M., Carreras, J., Dahmani, A., Debat, P., Driouch, Y., Druet, E., Guitard, G., Liesa, M., Mercier, A., Pouget, P., Reche-Estrada, J., Roux, L., Vaquer, R., 1996. Métamorphisme hercynienne. In: Barnolas, A., Chiron, J.C. (eds.). Synthèse Géologique et Géophysique des Pyrénées, tome 1 – Cycle Hercynien. BRGM-ITGE, 501-584. Gutiérrez-Alonso, G., Fernández-Suárez, J., Jeffries, T.E., 2004. Age and setting of the Upper Neoproterozoic Narcea Antiform volcanic rocks (NW Iberia). Geogaceta, 25, 79-82.

Hanson, G.N., Langmuir, C.H., 1978. Modelling of major elements in mantle-melt systems using trace element approaches. Geochimica et Cosmochimica Acta, 42(6), 725-741. DOI: https://doi.org/10.1016/0016-7037(78)90090-X

Hawthorne, F.C., Oberti, R., Harlow, G.E., Maresch, W.V., Martin, R.F., Schumacher, J.C., Welch, M.D., 2012. IMA report: Nomenclature of the amphibole supergroup. American Mineralogist, 97, 2031-2048. DOI: https://doi.org/10.2138/am.2012.4276

Hey, M.H., 1954. A new review of the chlorites. Mineralogical Magazine, 30, 277-292. DOI: https://doi.org/10.1180/minmag.1954.030.224.01

Holland, T.J.B., Powell, R., 1998. An internally consistent thermodynamic data set for phases of petrological interest. Journal of Metamorphic Geology, 16, 309-343. https://doi.org/10.1111/j.1525-1314.1998

Irvine, T.N., Baragar, W.R.A., 1971. A guide to the chemical classification of the common volcanic rocks. Canadian Journal of Earth Sciences, 8(5), 523–548. DOI: https://doi.org/10.1139/E71-055

Ishizuka, O., Tani, K., Reagan, M.K., Kanayama, K., Umino, S., Harigane, Y., Sakamoto, I., Miyajima, Y., Yuasa, M., Dunkley, D.J., 2011. The timescales of subduction initiation and subsequent evolution of an oceanic island arc. Earth and Planetary Science Letters, 306(3-4), 229-240. DOI: https://doi.org/10.1016/J.EPSL.2011.04.006

Jacobsen, S.B., Wasserburg, G.J., 1980. Sm-Nd isotopic evolution of chondrites. Earth and Planetary Science Letters, 50, 139-155. DOI: https://doi.org/10.1016/0012-821X(80)90125-9

Kroner, A., Stern, R.J., 2005. Pan-African Orogeny. Encyclopedia of Geology, 1-12. DOI: https://doi.org/10.1016/B0-12-369396-9/00431-7

Lázaro, C., García-Casco, A., Blanco-Quintero, I.F., Rojas-Agramonte, Y., Corsini, M., Proenza, J.A., 2015. Did the Turonian–Coniacian plume pulse trigger subduction initiation in the Northern Caribbean? Constraints from 40Ar/39Ar dating of the Moa-Baracoa metamorphic sole (eastern Cuba). International Geology Review, 57, 919-942. DOI: https://doi.org/10.1080/00206814.2014.924037

Leake, B.E., Wooley, A.R., Arps, C.E.S., Birch, W.D., Gilbert, M.C., Grice, J.D., Hawthorne, F.C., Kato, A., Kish, H.J., Krivovichev, V.G., Linthout, K., Laird, J., Mandarino, J.A., Maresch, W.V., Nickel, E.H., Rock, N.M.S., Schumacher, J.C., Smith, D.C., Stephenson, N.C.N., Ungaretti, L., Whittaker, E.J.W., Youzhi, G., 1997. Nomenclature of amphiboles; Report of the Subcommittee on Amphiboles of the International Mineralogical Association, Commission on New Minerals and Mineral Names. Mineralogical Magazine, 61(405), 295-310. DOI: https://doi.org/10.1180/minmag.1997.061.405.13

Liesa, M., Carreras, J., 1989. On the structure and metamorphism of the Roc de Frausa Massif, Eastern Pyrenees. Geodinamica Acta, 3(2), 149-161.

Liesa, M., Aguilar, C., Castro, A., Gisbert, G., Reche, J., Muñoz, J.A., Vilà, M., 2021. The role of mantle and crust in the generation of calc-alkaline Variscan magmatism and its tectonic setting in the Eastern Pyrenees. Lithos, 406-407, 106541. DOI: https://doi.org/10.1016/j.lithos.2021.106541

Losantos, M., Palau, J., Carreras, J., Druguet, E., Santanach, P., Cirés, J., 1997. Mapa geològic de Catalunya, Escala 1:25.000. Barcelona (España), Fulls: Roses 259-1-1, Cap de Creus, 259-2-1, Far de Roses 259-1-2, Institut Cartogràfic de Catalunya (ICC).

Lugmair, G.W., Marti, K., 1978. Lunar initial 143Nd/144Nd: Differential evolution of the lunar crust and mantle. Earth and Planetary Science Letters, 39, 349-357. DOI: https://doi.org/10.1016/0012-821X(78)90021-3

de Marien, L.H., Le Bayon, B., Pitra, P., Van Den Driessche, J., Poujol, M., Cagnard, F., 2019. Two-stage Variscan metamorphism in the Canigou massif: Evidence for crustal thickening in the Pyrenees. Journal of Metamorphic Geology, 37(6), 863-888. DOI: https://doi.org/10.1111/jmg.12487

Martínez, F.J., Rolet, J., 1988. Late Paleozoic metamorphism in the Northwestern Iberian Peninsula, Brittany and related areas in South-West Europe. In: Harris, I.J., Fettes, D.J. (eds.). The Caledonian-Appalachian Orogen. London, The Geological Society, 38(1, Special Publications), 611-620. DOI: https://doi.org/10.1144/GSL.SP.1988.038.01.42

Martínez, F.J., Dietsch, C., Aleinikoff, J., Cirés, J., Arboleya, M.L., Reche, J., Gómez-Gras, D., 2016. Provenance, age, and tectonic evolution of Variscan flysch, southeastern France and northeastern Spain, based on zircon geochronology. Geological Society of America Bulletin, 128, 842-859. DOI: https://doi.org/10.1130/B31316.1

Matte, P., Mattauer, M., 1987. Hercynian orogeny in the Pyrenees was not a rifting event. Nature, 325, 739-740. DOI: https://doi.org/10.1038/325739b0

Meert, J.G., Lieberman, B.S., 2008. The Neoproterozoic assembly of Gondwana and its relationship to the Ediacaran–Cambrian radiation. Gondwana Research, 14(1-2), 5-21. DOI: https://doi.org/10.1016/J.GR.2007.06.007

Mezger, J.E., 2010. Cadomian, Ordovician and Variscan igneous events preserved in gneiss domes of the Central Pyrenean Axial Zone. 13. Symposium "Tektonik, Struktur- und Kristallingeologie" (TSK 13), Frankfurt, April 6-12, 2010, Conference abstracts and field guides, 40.

Mezger, J., Gerdes, A., 2016. Early Variscan (Visean) granites in the core of central Pyrenean gneiss domes: implications from laser ablation U–Pb and Th–Pb studies. Gondwana Research, 29, 181-198. DOI: https://doi.org/10.1016/j.gr.2014.11.010

Micheletti, F., Barbey, P., Fornelli, A., Piccarreta, G., Deloule, E., 2007. Latest Precambrian to Early Cambrian U-Pb zircon ages of augen gneisses from Calabria (Italy), with inference to the Alboran microplate in the evolution of the peri-Gondwana terranes. International Journal of Earth Sciences, 96, 843-860. DOI: https://doi.org/10.1007/s00531-006-0136-0

Moghadam, H.S., Khademi, M., Hu, Z., Stern, R.J., Santos, J.F., Wu, Y., 2015. Cadomian (Ediacaran–Cambrian) arc magmatism in the ChahJam–Biarjmand metamorphic complex (Iran): magmatism along the northern active margin of Gondwana. Gondwana Research, 27, 439-452. DOI: https://doi.org/10.1016/j.gr.2013.10.014

Moghadam, H.S., Griffin, W.L., Li, X.H., Santos, J.F., Karsli, O., Stern, R.J., Ghorbani, G., Gain, S., Murphy, R., O'Reilly, S.Y., 2017. Crustal evolution of NW Iran: Cadomian arcs, Archean fragments and the Cenozoic magmatic flare-up. Journal of Petrology, 58(11), 2143-2190. DOI: https://doi.org/10.1093/petrology/egy005

Montero, P., Bea, F., 1998. Accurate determination of 87Rb/86Sr and 147Sm/144Nd ratios by inductively-coupled-plasma mass spectrometry in isotope geoscience: An alternative to isotope dilution analysis. Analytica Chimica Acta, 358, 227-233. DOI: https://doi.org/10.1016/S0003-2670(97)00599-0

Muñoz, J.A., 1992. Evolution of a continental collision belt: ECORS-Pyrenees crustal balanced cross-section. In: Mc Clay, K.R. (eds.). Thrust Tectonics. London, Chapman & Hall, 235-246.

Nance, R.D., Gutiérrez-Alonso, G., Keppie, J.D., Linnemann, U., Murphy, J.B., Quesada, C., Strachan, R.A., Woodcock, N.H., 2010. Evolution of the Rheic Ocean. Gondwana Research, 17(2-3), 194-222. DOI: https://doi.org/10.1016/J.GR.2009.08.001

Navidad, M., Carreras, J., 1995. Pre-Hercynian magmatism in the eastern Pyrenees (Cap de Creus and Albera Massifs) and its geodynamical setting. Geologie en Mijnbouw, 74, 65-77.

Navidad, M., Carreras, J., 2002. El volcanismo de la base del Paleozoico Inferior del Canigó (Pirineos Orientales). Evidencias geoquímicas de la apertura de una cuenca continental. Geogaceta, 32, 91-94.

Navidad, M., Castiñeiras, P., Casas, J.M., Liesa, M., Fernández Suárez, J., Barnolas, A., Carreras, J., Gil-Peña, I., 2010. Geochemical characterization and isotopic age of Caradocian magmatism in the northeastern Iberian Peninsula: Insights into the Late Ordovician evolution of the northern Gondwana margin. Gondwana Research, 17, 325-337. DOI: https://doi.org/10.1016/j.gr.2009.11.013

Navidad, M., Castiñeiras, P., Casas, J.M., Liesa, M., Belousova, E., Proenza, J., Aiglsperger, T., 2018. Ordovician magmatism in the Eastern Pyrenees: Implications for the geodynamic evolution of northern Gondwana. Lithos, 314-315, 479-496. DOI: https://doi.org/10.1016/J.LITHOS.2018.06.019

Ouabid, M., Garrido, C.J., Ouali, H., Harvey, J., Hidas, K., Marchesi, C., Acosta-Vigil, A., Dautria, J.M., el Messbahi, H., Román-Alpiste, M.J., 2020. Late Cadomian rifting of the NW Gondwana margin and the reworking of Precambrian crust – evidence from bimodal magmatism in the early Paleozoic Moroccan Meseta. International Geology Review, 63(16), 2013-2036. DOI: https://doi.org/10.1080/00206814.2020.1818301

Padel, M., Álvaro, J.J., Casas, J.M., Clausen, S., Poujol, M., Sánchez-García, T., 2018a. Cadomian volcanosedimentary complexes across the Ediacaran–Cambrian transition of the Eastern Pyrenees, southwestern Europe. International Journal of Earth Sciences, 107, 1579-1601. DOI: https://doi.org/10.1007/S00531-017-1559-5

Padel, M., Clausen, S., Álvaro, J.J., Casas, J.M., 2018b. Review of the Ediacaran–Lower Ordovician (pre–Sardic) stratigraphic framework of the Eastern Pyrenees, southwestern Europe. Geologica Acta, 16(4), 339-355.

DePaolo, D.J., Wasserburg, G.J., 1976. Nd isotopic variations and petrogenetic models. Geophysical Research Letters, 3, 249-252. DOI: https://doi.org/10.1029/GL003I005P00249

DePaolo, D.J., 1981. Neodymium isotopes in the Colorado Front Range and crust–mantle evolution in the Proterozoic. Nature, 291, 193-196. DOI: https://doi.org/10.1038/291193a0

Paton, C., Hellstrom, J., Paul, B., Woodhead, J., Hergt, J., 2011. Iolite: Freeware for the visualisation and processing of mass spectrometric data. Journal of Analytical Atomic Spectrometry, 26, 2508-2518. DOI: https://doi.org/10.1039/C1JA10172B

Pearce, J.A., 1996. Sources and setting of granitic rocks. Episodes, 19(4), 120-125. DOI: https://doi.org/10.18814/epiiugs/1996/v19i4/005

Pearce, J.A., 2008. Geochemical fingerprinting of oceanic basalts with applications to ophiolite classification and the search for Archean oceanic crust. Lithos, 100, 14-48. DOI: https://doi.org/10.1016/J.LITHOS.2007.06.016

Pearce, J.A., 2014. Immobile element fingerprinting of ophiolites. Elements, 10(2), 101-108. DOI: https://doi.org/10.2113/gselements.10.2.101

Pereira, M., Castro, A., Chichorro, M., Fernández, C., Díaz-Alvarado, J., Martí, J., Rodríguez, C., 2014. Chronological link between deep-seated processes in magma chambers and eruptions: Permo–Carboniferous magmatism in the core of Pangaea (Southern Pyrenees). Gondwana Research, 25, 290-308. DOI: https://doi.org/10.1016/j.gr.2013.03.009

Pouchou, J.L., Pichoir, F., 1991. Quantitative Analysis of Homogeneous or Stratified Microvolumes Applying the Model "PAP." Electron Probe Quantitation, 31-75. DOI: https://doi.org/10.1007/978-1-4899-2617-3_4

Powell, R., Holland, T.J.B., 1994. Optimal geothermometry and geobarometry. American Mineralogist, 79, 120-133.

von Raumer, J.F., Stampfli, G.M., 2008. The birth of the Rheic Ocean — Early Palaeozoic subsidence patterns and subsequent tectonic plate scenarios. Tectonophysics, 461(1-4), 9-20. DOI: https://doi.org/10.1016/J.TECTO.2008.04.012

von Raumer, J.F., Stampfli, G.M., Arenas, R., Sánchez Martínez, S., 2015. Ediacaran to Cambrian oceanic rocks of the Gondwana margin and their tectonic interpretation. International Journal of Earth Sciences, 104, 1107-1121. DOI: https://doi.org/10.1007/S00531-015-1142-X

Reagan, M.K., Ishizuka, O., Stern, R.J., Kelley, K.A., Ohara, Y., Blichert-Toft, J., Bloomer, S.H., Cash, J., Fryer, P., Hanan, B.B., Hickey-Vargas, R., Ishii, T., Kimura, J.I., Peate, D.W., Rowe, M.C., Woods, M., 2010. Fore-arc basalts and subduction initiation in the Izu-Bonin-Mariana system. Geochemistry, Geophysics, Geosystems, 11(3), 1-17. DOI: ttps://doi.org/10.1029/2009GC002871

Reche, J., Carreras, J., Druguet, E., 1996. Métamorphisme Hercynien: Le massif du Cap de Creus. In: Barnolas, A., Chiron, J.C. (eds.). Synthèse géologique et gèophisique des Pyrénées. Orleans-Madrid, Bureau de Recherches Géologiques et Minières - Instituto Tecnológico Geominero de España, 1, 524-530.

Ribeiro, M.L., Reche, J., López-Carmona, A., Aguilar, C., Bento dos Santos, T., Chichorro, M., Dias da Silva, Í., Díez-Montes, A., González-Clavijo, E., Gutiérrez-Alonso, G., Leal, N., Liesa, M., Martínez, F.J., Mateus, A., Mendes, M.H., Moita, P., Pedro, J., Quesada, C., Santos, J.F., Solá, A.R., Valverde-Vaquero, P., 2019. Variscan Metamorphism. In: Quesada, C., Oliveira, J. (eds.). The Geology of Iberia: A Geodynamic Approach. Regional Geology Reviews. Springer, Cham, 431-495. DOI: https://doi.org/10.1007/978-3-030-10519-8_12

Rodriguez-Corcho, A.F., Rojas-Agramonte, Y., Barrera-Gonzalez, J.A., Marroquin-Gomez, M.P., Bonilla-Correa, S., Izquierdo-Camacho, D., Delgado-Balaguera, S.M., Cartwright-Buitrago, D., Muñoz-Granados, M.D., Carantón-Mateus, W.G., Corrales-García, A., Laverde-Martinez, A.F., Cuervo-Gómez, A., Rodriguez-Ruiz, M.A., Marin-Jaramillo, J.P., Salazar-Cuellar, N., Esquivel-Arenales, L.C., Daroca, M.E., Carvajal, A.S., Perea-Pescadora, A.M., Solano-Acosta, J.D., Diaz, S., Guillen, A., Bayona, G., Cardona-Molina, A., Eglington, B., Montes, C., 2020. The Colombian geochronological database (CGD). International Geology Review, 64(12), 1635-1669. DOI: https://doi.org/10.1080/00206814.2021.1954556

Rodriguez-Corcho, A.F., actions-user, 2021. andresrcorcho/CGD_HistogramsApp: HistogramsApp_1.3 (Version 1.3): Zenodo. DOI: https://doi.org/10.5281/zenodo.4593488

Rojo-Pérez, E., Arenas, R., Fuenlabrada, J.M., Sánchez Martínez, S., Martín Parra, L.M., Matas, J., Pieren, A.P., Díez Fernández, R., 2019. Contrasting isotopic sources (Sm-Nd) of Late Ediacaran series in the Iberian Massif: Implications for the Central Iberian-Ossa Morena boundary. Precambrian Research, 324, 194-207. DOI: https://doi.org/10.1016/J.PRECAMRES.2019.01.021

Rojo-Pérez, E., Fuenlabrada, J.M., Linnemann, U., Arenas, R., Sánchez Martínez, S., Díez Fernández, R., Martín Parra, L.M., Matas, J., Andonaegui, P., Fernández-Suárez, J., 2021. Geochemistry and Sm–Nd isotopic sources of Late Ediacaran siliciclastic series in the Ossa–Morena Complex: Iberian–Bohemian correlations. International Journal of Earth Sciences, 110(2), 467-485. DOI: https://doi.org/10.1007/s00531-020-01963-0

Rojo-Pérez, E., Linnemann, U., Hofmann, M., Fuenlabrada, J.M., Zieger, J., Fernández-Suárez, J., Andonaegui, P., Sánchez Martínez, S., Díez Fernández, R., Arenas, R., 2022. U-Pb geochronology and isotopic geochemistry of adakites and related magmas in the Ediacaran arc section of the SW Iberian Massif: The role of subduction erosion cycles in peri-

Gondwanan arcs. Gondwana Research, 109, 89-112. DOI: https://doi.org/10.1016/J.GR.2022.04.011

Ross, P.S., Bédard, J.H., 2009. Magmatic affinity of modern and ancient subalkaline volcanic rocks determined from trace-element discriminant diagrams. Canadian Journal of Earth Sciences, 46(11), 823-839. DOI: https://doi.org/10.1139/E09-054

Rubio-Ordóñez, A., Gutiérrez-Alonso, G., Valverde-Vaquero, P., Cuesta, A., Gallastegui, G., Gerdes, A., Cárdenes, V., 2015. Arc-related Ediacaran magmatism along the northern margin of Gondwana: Geochronology and isotopic geochemistry from northern Iberia. Gondwana Research, 27, 216-227. DOI: https://doi.org/10.1016/J.GR.2013.09.016

Sánchez-Lorda, M.E., Sarrionandia, F., Ábalos, B., Carrracedo, M., Eguíluz, L., Gil-Ibarguchi, J.I., 2014. Geochemistry and paleotectonic setting of Ediacaran metabasites from the Ossa-Morena Zone (SW Iberia). International Journal of Earth Sciences, 103, 1263-1286. DOI: https://doi.org/10.1007/S00531-013-0937-X

Sánchez-Lorda, M.E., Ábalos, B., García de Madinabeitia, S., Eguíluz, L., Gil-Ibarguchi, J.I., Paquette, J.L., 2016. Radiometric discrimination of pre-Variscan amphibolites in the Ediacaran Serie Negra (Ossa-Morena Zone, SW Iberia). Tectonophysics, 681, 31-45. DOI: https://doi.org/10.1016/J.TECTO.2015.09.020

Santanach, P.F., 1972. Estudio tectónico del Paleozoico inferior del Pirineo entre la Cerdaña y el río Ter. Acta Geologica Hispanica, 7(2), 44-49.

Shervais, J.W., 2022. The petrogenesis of modern and ophiolitic lavas reconsidered: Ti-V and Nb-Th. Geoscience Frontiers, 13(2), 101319. DOI: https://doi.org/10.1016/J.GSF.2021.101319

Sláma, J., Košler, J., Pedersen, R.B., 2008. Behaviour of zircon in high-grade metamorphic rocks: evidence from Hf isotopes, trace elements and textural studies. Contributions to Mineralogy and Petrology, 154(3), 335-356. DOI: https://doi.org/10.1007/s00410-007-0196-6

Soula, J.C., 1982. Characteristics and mode of emplacement of gneiss domes and plutonic domes in central-eastern Pyrenees. Journal of Structural Geology, 4(3), 313-342. DOI: https://doi.org/10.1016/0191-8141(82)90017-7

Spear, F.S., 1993. Metamorphic phase equilibria and pressure-temperature-time paths. Washington DC, Mineralogical Society of America. 799p.

Sun, S.S., McDonough, W.F., 1989. Chemical and isotopic systematics of oceanic basalts: implications for mantle composition and processes. London, The Geological Society, 42(1, Special Publications), 313-345. DOI: https://doi.org/10.1144/GSL.SP.1989.042.01.19

Tanaka, T., Togashi, S., Kamioka, H., Amakawa, H., Kagami, H., Hamamoto, T., Yuhara, M., Orihashi, Y., Yoneda, S., Shimizu, H., Kunimaru, T., Takahashi, K., Yanagi, T., Nakano, T., Fujimaki, H., Shinjo, R., Asahara, Y., Tanimizu, M., Dragusanu, C., 2000. JNdi-1: a neodymium isotopic reference in consistency with La Jolla neodymium. Chemical Geology, 168, 279-281. DOI: https://doi.org/10.1016/S0009-2541(00)00198-4

Torró, L., Proenza, J.A., Marchesi, C., Garcia-Casco, A., Lewis, J.F., 2017. Petrogenesis of meta-volcanic rocks from the Maimón Formation (Dominican Republic): Geochemical record of the nascent Greater Antilles paleo-arc. Lithos, 278-281, 255-273. DOI: https://doi.org/10.1016/j.lithos.2017.01.031

Tournaire Guille, B., Olivier, P., Paquette, J.-L., Bosse, V., Guillaume, D., 2019. Evolution of the middle crust of the Pyrenees during the Paleozoic: new data on the plutonic rocks from the North Pyrenean Agly Massif. International Journal of Earth Sciences, 108, 245-265. DOI: https://doi.org/10.1007/s00531-018-1652-4

Villaseca, C., Castiñeiras, P., Orejana, D., 2015. Early Ordovician metabasites from the Spanish Central System: A remnant of intraplate HP rocks in the Central Iberian Zone. Gondwana Research, 27, 392-409. DOI: https://doi.org/10.1016/J.GR.2013.10.007

Villaseca, C., Orejana, D., Higueras, P., Pérez-Soba, C., García Serrano, J., Lorenzo, S., 2022. The evolution of the subcontinental mantle beneath the Central Iberian Zone: Geochemical tracking of its mafic magmatism from the Neoproterozoic to the Cenozoic. Earth-Science Reviews, 228, 103997. DOI: https://doi.org/10.1016/J.EARSCIREV.2022.103997

Whitney, D.L., Evans, B.W., 2010. Abbreviations for names of rock-forming minerals. American Mineralogist, 95, 185-187. DOI: https://doi.org/10.2138/am.2010.3371

Wiedenbeck, M., Allé, P., Corfu, F., Griffin, W.L., Meier, M., Oberli, F., von Quadt, A., Roddick, J.C., Spiegel, W., 1995. Three natural zircon standards for U-Th-Pb, Lu-Hf, trace element and REE analyses. Geostandards Newsletter, 19(1), 1-23. DOI: https://doi.org/10.1111/J.1751-908X.1995.TB00147.X

Williams, I.S., Fiannacca, P., Cirrincione, R., Pezzino, A., 2012. Peri-Gondwanan origin and early geodynamic history of NE Sicily: A zircon tale from the basement of the Peloritani Mountains. Gondwana Research, 22, 855-865. DOI: https://doi.org/10.1016/j.gr.2011.12.007

Winchester, J.A., Floyd, P.A., 1977. Geochemical discrimination of different magma series and their differentiation products using immobile elements. Chemical Geology, 20, 325-343. DOI: https://doi.org/10.1016/0009-2541(77)90057-2

Wood, D.A., 1980. The application of a ThHfTa diagram to problems of tectonomagmatic classification and to establishing the nature of crustal contamination of basaltic lavas of the British Tertiary Volcanic Province. Earth and Planetary Science Letters, 50, 11-30. DOI: https://doi.org/10.1016/0012-821X(80)90116-8

Yilmaz Şahin, S., Aysal, N., Güngör, Y., Peytcheva, I., Neubauer, F., 2013. Geochemistry and U–Pb zircon geochronology of metagranites in Istranca (Strandja) Zone, NW Pontides, Turkey: Implications for the geodynamic evolution of Cadomian orogeny. Gondwana Research, 26, 755-771. DOI: http://dx.doi.org/10.1016/j.gr.2013.07.011

Zwart, H.J., 1962. On the determination of polymetamorphic mineral associations, and its application to the Bosost Area (Central Pyrenees). Geologische Rundschau, 52(1), 38-65. DOI: https://doi.org/10.1007/BF01840064

Zwart, H.J., 1979. The Geology of the Central Pyrenees. Leidse Geologische Mededelingen, 50, 1-74.

Manuscript received March 2022;
revision accepted October 2022;
published Online November 2022.

APPENDIX I

Representative electron probe microanalyses (EPMA) of the different minerals in the studied metabasites

Table I. Amphibole

Sample	CG-18-01	CG-18-01	CG-18-04	CG-18-04	CC-18-01	CC-18-01	CC-18-01	CC-18-02	CC-18-02	CC-18-03	CC-18-03	CC-18-03
Massif	Canigó	Canigó	Canigó	Canigó	Cap de Creus	Cap de Creus	Cap de Creus	Cap de Creus	Cap de Creus	Cap de Creus	Cap de Creus	Cap de Creus
Mineral	Amp	Amp	Amp	Amp	Amp	Amp	Amp	Amp	Amp	Amp	Amp	Amp
SiO_2	52.43	54.55	50.03	53.02	51.32	43.54	45.42	49.68	45.90	42.50	50.32	47.09
TiO_2	0.03	0.04	0.10	0.05	0.05	0.43	0.38	0.11	0.41	0.47	0.12	0.29
Al_2O_3	2.77	1.95	5.29	2.76	3.00	11.26	9.46	3.85	8.53	12.17	3.82	8.06
Cr_2O_3	0.00	0.06	0.21	0.00	0.04	0.04	0.04	0.00	0.00	0.15	0.12	0.10
FeO	11.36	10.25	14.24	13.07	13.90	16.27	15.33	19.04	20.36	18.72	15.77	16.72
MnO	0.23	0.22	0.28	0.26	0.26	0.25	0.26	0.27	0.24	0.31	0.28	0.30
MgO	16.56	17.52	13.09	14.90	14.64	10.30	11.30	11.03	8.76	8.65	13.32	11.07
NiO	0.07	0.00	0.01	0.05	0.00	0.02	0.05	0.00	0.00	0.00	0.00	0.00
CaO	12.53	12.70	12.07	12.40	12.11	11.98	11.94	11.31	11.19	11.30	11.80	11.57
Na_2O	0.26	0.25	0.49	0.25	0.34	1.30	1.04	0.55	1.05	1.38	0.40	0.82
K_2O	0.06	0.04	0.20	0.09	0.07	0.46	0.25	0.16	0.22	0.27	0.05	0.14
Total	96.31	97.58	96.02	96.85	95.74	95.84	95.47	96.00	96.65	95.93	96.00	96.15
Si	7.58	7.74	7.40	7.70	7.55	6.57	6.82	7.49	6.94	6.45	7.45	7.02
Ti	0.00	0.00	0.01	0.01	0.01	0.05	0.04	0.01	0.05	0.05	0.01	0.03
Al	0.47	0.33	0.92	0.47	0.52	2.00	1.67	0.68	1.52	2.18	0.67	1.42
Cr	0.00	0.01	0.02	0.00	0.00	0.00	0.01	0.00	0.00	0.02	0.01	0.01
Fe^{3+}	0.33	0.16	0.14	0.10	0.34	0.35	0.32	0.29	0.36	0.51	0.38	0.35
Fe^{2+}	1.04	1.05	1.62	1.49	1.37	1.70	1.61	2.11	2.22	1.87	1.57	1.73
Mn	0.03	0.03	0.04	0.03	0.03	0.03	0.03	0.03	0.03	0.04	0.04	0.04
Mg	3.57	3.71	2.89	3.23	3.21	2.32	2.53	2.48	1.97	1.96	2.94	2.46
Ni	0.01	0.00	0.00	0.01	0.00	0.00	0.01	0.00	0.00	0.00	0.00	0.00
Ca	1.94	1.93	1.91	1.93	1.91	1.94	1.92	1.83	1.81	1.84	1.87	1.85
Na	0.07	0.07	0.14	0.07	0.10	0.38	0.30	0.16	0.31	0.41	0.11	0.24
K	0.01	0.01	0.04	0.02	0.01	0.09	0.05	0.03	0.04	0.05	0.01	0.03
#Mg	0.77	0.78	0.64	0.68	0.70	0.58	0.61	0.54	0.47	0.51	0.65	0.59

Table II. Plagioclase

Sample	CG-18-01	CG-18-01	CG-18-04	CG-18-04	CC-18-01	CC-18-01	CC-18-02	CC-18-03	CC-18-03	CC-18-03
Massif	Canigó	Canigó	Canigó	Canigó	Cap de Creus	Cap de Creus	Cap de Creus	Cap de Creus	Cap de Creus	Cap de Creus
Mineral	Pl	Pl	Pl	Pl	Pl	Pl	Pl	Pl	Pl	Pl
SiO_2	67.00	64.28	64.04	66.81	63.97	56.45	67.40	63.50	61.45	65.91
TiO_2	0.00	0.00	0.00	0.00	0.00	0.00	0.00	0.00	0.03	0.09
Al_2O_3	20.08	21.09	21.54	20.09	22.07	26.79	20.44	21.66	23.15	20.95
Cr_2O_3	0.01	0.00	0.00	0.02	0.01	0.00	0.00	0.10	0.04	0.00
FeO	0.41	0.39	0.18	0.21	0.26	0.21	0.11	0.32	0.27	0.24
MnO	0.00	0.00	0.00	0.00	0.02	0.00	0.03	0.00	0.01	0.00
MgO	0.05	0.02	0.00	0.01	0.02	0.01	0.00	0.00	0.01	0.01
NiO	0.03	0.00	0.02	0.00	0.01	0.04	0.00	0.01	0.01	0.00
CaO	0.70	2.02	2.51	0.90	3.00	8.63	0.84	2.75	4.32	1.60
Na_2O	11.63	10.01	10.72	11.58	9.08	6.75	11.65	10.01	8.92	11.06
K_2O	0.04	0.07	0.08	0.08	0.06	0.06	0.06	0.03	0.04	0.05
Total	99.95	97.88	99.09	99.70	98.49	98.94	100.53	98.39	98.25	99.91
Si	2.94	2.88	2.85	2.94	2.85	2.56	2.94	2.85	2.77	2.90
Ti	0.00	0.00	0.00	0.00	0.00	0.00	0.00	0.00	0.00	0.00
Al	1.04	1.12	1.13	1.04	1.16	1.43	1.05	1.14	1.23	1.09
Cr	0.00	0.00	0.00	0.00	0.00	0.00	0.00	0.00	0.00	0.00
Fe^{3+}	0.02	0.01	0.01	0.01	0.01	0.01	0.00	0.01	0.01	0.01
Fe^{2+}	0.00	0.00	0.00	0.00	0.00	0.00	0.00	0.00	0.00	0.00
Mn	0.00	0.00	0.00	0.00	0.00	0.00	0.00	0.00	0.00	0.00
Mg	0.00	0.00	0.00	0.00	0.00	0.00	0.00	0.00	0.00	0.00
Ni	0.00	0.00	0.00	0.00	0.00	0.00	0.00	0.00	0.00	0.00
Ca	0.03	0.10	0.12	0.04	0.14	0.42	0.04	0.13	0.21	0.08
Na	0.99	0.87	0.93	0.99	0.79	0.59	0.99	0.87	0.78	0.94
K	0.00	0.00	0.00	0.00	0.00	0.00	0.00	0.00	0.00	0.00
Ab	0.97	0.90	0.88	0.95	0.84	0.58	0.96	0.87	0.79	0.92
An	0.03	0.10	0.11	0.04	0.15	0.41	0.04	0.13	0.21	0.07
Or	0.00	0.00	0.00	0.00	0.00	0.00	0.00	0.00	0.00	0.00

Table III. Chlorite

Massif	Canigó	Canigó	Canigó	Canigó	Cap de Creus	Cap de Creus	Cap de Creus
Mineral	Chl	Chl	Chl	Chl	Chl	Chl	Chl
SiO_2	26.48	25.97	24.87	25.49	24.54	24.10	24.77
TiO_2	0.00	0.00	0.00	0.04	0.10	0.05	1.00
Al_2O_3	19.90	20.82	20.55	20.20	20.58	20.47	20.65
Cr_2O_3	0.27	0.04	0.13	0.16	0.00	0.08	0.00
FeO	19.84	20.27	23.48	23.43	22.43	22.08	29.96
MnO	0.29	0.30	0.28	0.29	0.27	0.28	0.24
MgO	19.13	18.93	16.26	16.48	16.54	16.59	11.79
NiO	0.02	0.10	0.00	0.04	0.00	0.05	0.01
CaO	0.23	0.04	0.08	0.03	0.13	0.13	0.04
Na_2O	0.06	0.00	0.00	0.03	0.02	0.05	0.05
K_2O	0.05	0.01	0.01	0.01	0.08	0.04	0.34
Total	86.28	86.48	85.67	86.21	84.68	83.92	88.84
Si	5.53	5.41	5.34	5.43	5.31	5.26	5.31
Ti	0.00	0.00	0.00	0.01	0.02	0.01	0.16
Al	4.89	5.11	5.20	5.07	5.25	5.27	5.21
Cr	0.05	0.01	0.02	0.03	0.00	0.01	0.00
Fe^{2+}	3.46	3.53	4.21	4.17	4.06	4.03	5.37
Mn	0.05	0.05	0.05	0.05	0.05	0.05	0.04
Mg	5.95	5.88	5.20	5.23	5.33	5.40	3.77
Ni	0.00	0.02	0.00	0.01	0.00	0.01	0.00
Ca	0.05	0.01	0.02	0.01	0.03	0.03	0.01
Na	0.02	0.00	0.00	0.01	0.01	0.02	0.02
K	0.01	0.00	0.00	0.00	0.02	0.01	0.09
#Mg	0.63	0.62	0.55	0.56	0.57	0.57	0.41

Table IV. Epidote

Sample	CG-18-01	CG-18-01	CG-18-04	CG-18-04	CC-18-01	CC-18-01
Massif	Canigó	Canigó	Canigó	Canigó	Cap de Creus	Cap de Creus
Mineral	Ep	Ep	Ep	Ep	Ep	Ep
SiO_2	38.28	38.29	38.12	38.64	37.54	37.90
TiO_2	0.03	0.00	0.18	0.04	0.11	0.10
Al_2O_3	28.17	28.99	27.37	29.90	27.71	27.54
Cr_2O_3	0.08	0.18	0.13	0.01	0.06	0.00
FeO	5.80	4.27	6.56	3.76	5.83	6.26
MnO	0.12	0.08	0.12	0.06	0.15	0.11
MgO	0.04	0.03	0.03	0.00	0.04	0.05
NiO	0.03	0.00	0.02	0.00	0.04	0.00
CaO	23.55	23.72	23.42	23.99	23.26	23.70
Na_2O	0.02	0.00	0.01	0.00	0.10	0.02
K_2O	0.00	0.01	0.00	0.00	0.10	0.00
Suma	96.12	95.57	95.96	96.40	94.94	95.69
Si	3.01	3.01	3.01	3.01	2.99	3.00
Ti	0.00	0.00	0.01	0.00	0.01	0.01
Al	2.61	2.69	2.54	2.74	2.60	2.57
Cr	0.00	0.01	0.01	0.00	0.00	0.00
Fe^{3+}	0.38	0.28	0.43	0.24	0.39	0.41
Mn	0.01	0.01	0.01	0.00	0.01	0.01
Mg	0.00	0.00	0.00	0.00	0.00	0.01
Ni	0.00	0.00	0.00	0.00	0.00	0.00
Ca	1.98	2.00	1.98	2.00	1.99	2.01
Na	0.00	0.00	0.00	0.00	0.01	0.00
K	0.00	0.00	0.00	0.00	0.01	0.00
Xpist	0.39	0.29	0.44	0.25	0.39	0.42

Table V. Accessory minerals: titanite, ilmenite, rutile, biotite, and magnetite

Sample	CG-18-01	CG-18-04	CG-18-04	CG-18-04	CC-18-01	CC-18-01	CC-18-01	CC-18-03	CC-18-03
Massif	Canigó	Canigó	Canigó	Canigó	Cap de Creus	Cap de Creus	Cap de Creus	Cap de Creus	Cap de Creus
Mineral	Ttn	Ttn	Ilm	Rt	Ttn	Ilm	Bt	Mt	Ilm
SiO_2	29.97	30.97	0.04	0.06	29.59	0.02	46.01	0.06	0.15
TiO_2	38.55	35.17	52.01	91.67	37.92	53.35	0.18	0.04	51.97
Al_2O_3	1.24	1.93	0.00	0.03	1.03	0.02	30.47	0.00	0.02
Cr_2O_3	0.00	0.21	0.01	0.00	0.14	0.06	0.00	0.12	0.01
FeO	0.39	1.16	41.93	6.15	0.20	41.07	2.65	92.78	42.09
MnO	0.02	0.04	4.67	0.66	0.07	2.70	0.05	0.05	1.88
MgO	0.02	0.72	0.17	0.06	0.02	0.26	2.46	0.00	0.17
NiO	0.01	0.00	0.00	0.00	0.00	0.00	0.02	0.00	0.00
CaO	27.86	27.07	0.11	0.19	28.03	0.34	0.08	0.02	0.27
Na_2O	0.00	0.02	0.04	0.03	0.08	0.05	0.23	0.00	0.00
K_2O	0.00	0.01	0.00	0.00	0.05	0.01	8.41	0.08	0.00
Suma	98.05	97.30	98.98	98.86	97.12	97.87	90.56	93.15	96.56
Si	1.00	1.04	0.00	0.00	1.00	0.00	6.42	0.00	0.00
Ti	0.96	0.88	1.00	0.96	0.96	1.02	0.02	0.00	1.01
Al	0.05	0.08	0.00	0.00	0.04	0.00	5.01	0.00	0.00
Cr	0.00	0.01	0.00	0.00	0.00	0.00	0.00	0.00	0.00
Fe^{3+}	0.00	0.00	0.00	0.00	0.00	0.00	0.00	1.99	0.00
Fe^{2+}	0.01	0.03	0.89	0.07	0.01	0.87	0.31	0.99	0.91
Mn	0.00	0.00	0.10	0.01	0.00	0.06	0.01	0.00	0.04
Mg	0.00	0.04	0.01	0.00	0.00	0.01	0.51	0.00	0.01
Ni	0.00	0.00	0.00	0.00	0.00	0.00	0.00	0.00	0.00
Ca	0.99	0.97	0.00	0.00	1.01	0.01	0.01	0.00	0.01
Na	0.00	0.00	0.00	0.00	0.00	0.00	0.06	0.00	0.00
K	0.00	0.00	0.00	0.00	0.00	0.00	1.50	0.00	0.00

TABLE VI. U/Pb isotopic data for the Canigó chlorite-rich schist sample (CG-18-02) and the Cap de Creus metabasite sample (CC-18-02). U-Pb-Th values (ppm) are referenced to the 91500 zircon standard and hence these are taken as approximate concentrations

Sample	Spot_ID	U (ppm)	SD U (ppm)	Th (ppm)	SD Th (ppm)	Pb (ppm)	SD Pb (ppm)	Age 207/235	SD	Age 206/238	SD	Concordia Age	Conc. Error
CG-18-02 (75-100)	8590	133.50	3.30	177.80	4.10	57.20	2.75	694	19	610	10	605	10
CG-18-02 (75-100)	8591	170.30	4.50	114.10	2.70	37.20	1.70	699	15	609	18	661	14
CG-18-02 (75-100)	9711	133.00	6.50	108.50	4.60	37.30	2.25	753	13	713	16	741	13
CG-18-02 (75-100)	8596-30	92.00	3.25	70.00	2.15	50.00	2.25	1742	25	1500	35	1807	27
CG-18-02 (75-100)	8594	326.00	12.50	131.60	3.30	58.40	2.55	722	14	729	11	729	11
CG-18-02 (75-100)	8600	297.00	7.00	106.80	2.70	36.40	1.95	656	14	609	13	627	12
CG-18-02 (75-100)	8675	408.00	10.50	49.20	2.05	61.50	4.15	1891	18	1867	36	1903	15
CG-18-02 (75-100)	9322	1216.00	41.50	1400.00	60.00	635.00	32.00	2041	18	1882	36	2103	15
CG-18-02 (75-100)	9325	475.00	19.00	162.00	5.50	73.80	2.70	905	13	845	12	866	11
CG-18-02 (75-100)	8716-30	248.00	16.00	23.10	1.65	39.00	11.50	1925	25	1935	63	1922	19
CG-18-02 (75-100)	8697	132.90	4.45	275.00	8.00	132.00	5.50	837	18	805	24	829	18
CG-18-02 (75-100)	9712	2020.00	50.00	59.90	1.65	32.40	1.10	875	10	849	17	878	10
CG-18-02 (75-100)	8607	755.00	16.50	277.00	6.00	370.00	13.50	2407	17	2391	42	2414	12
CG-18-02 (75-100)	8606	644.00	16.50	142.10	3.95	109.00	5.00	1904	19	1627	41	2079	7
CG-18-02 (75-100)	8774	636.00	13.00	343.00	7.50	179.40	4.45	957	10	953	17	958	10
CG-18-02 (75-100)	8781	549.00	14.50	225.00	7.00	68.70	3.45	640	12	634	15	642	12
CG-18-02 (75-100)	8816	413.00	13.00	114.10	3.95	56.20	2.05	951	16	996	20	954	16
CG-18-02 (75-100)	9354	373.00	7.50	179.80	4.45	208.00	8.50	2456	18	2346	45	2490	15
CG-18-02 (75-100)	9364	280.00	8.50	405.00	8.50	112.30	4.20	668	11	624	13	651	10
CG-18-02 (75-100)	9539	1267.00	41.50	200.70	3.80	217.00	7.50	2504	14	2536	54	2496	10
CG-18-02 (75-100)	9541	1450.00	43.00	438.00	9.00	106.30	4.15	656	10	639	14	659	10
CG-18-02 (75-100)	9543	88.80	2.85	58.30	1.15	18.90	1.35	704	23	616	16	632	16
CG-18-02 (75-100)	9636	645.00	13.00	563.00	13.50	573.00	16.50	2535	19	2579	47	2517	14
CG-18-02 (75-100)	9645	182.00	6.00	73.30	2.30	23.20	1.35	700	18	693	16	695	15
CG-18-02 (75-100)	9649	2530.00	70.00	2200.00	48.00	790.00	30.00	809	8	808	14	810	8
CG-18-02 (75-100)	9650	131.10	2.70	109.90	3.75	57.00	2.60	1119	25	1105	22	1110	21
CG-18-02 (75-100)	9570	700.00	65.00	173.00	8.00	177.00	30.00	1961	24	2006	50	1928	13
CG-18-02 (75-100)	9572	124.70	2.10	79.50	1.10	97.10	2.90	2683	14	2771	28	2670	13

TABLE VI. Continued

Sample	Spot_ID	U (ppm)	SD U (ppm)	Th (ppm)	SD Th (ppm)	Pb (ppm)	SD Pb (ppm)	Age 207/235	SD	Age 206/238	SD	Concordia Age	Conc. Error
CG-18-02 (75-100)	9573	389.00	8.50	283.00	5.50	113.60	4.40	1041	11	1029	15	1039	11
CG-18-02 (75-100)	9577	91.90	2.75	23.20	0.95	9.20	0.55	906	27	915	21	913	20
CG-18-02 (75-100)	9585	645.00	14.50	626.00	13.00	236.00	10.00	816	9	817	10	816	8
CG-18-02 (75-100)	9579	471.00	11.00	1016.00	18.00	284.00	10.00	786	11	813	16	788	11
CG-18-02 (75-100)	9586	641.00	16.00	311.00	5.00	316.00	12.50	2530	15	2610	39	2499	11
CG-18-02 (75-100)	9578	150.40	4.35	185.30	3.65	53.30	2.00	687	16	699	14	694	12
CG-18-02 (75-100)	9575	202.00	7.00	120.40	3.00	39.20	1.90	814	13	822	19	815	13
CG-18-02 (75-100)	9450	894.00	38.00	203.00	10.50	135.00	22.00	753	36	596	19	575	18
CG-18-02 (75-100)	9269	45.10	4.35	37.70	3.85	19.60	3.90	897	30	822	28	853	24
CG-18-02 (75-100)	9723	1720.00	50.00	419.00	11.50	119.50	4.95	639	9	633	15	639	9
CG-18-02 (75-100)	9273	1064.00	23.50	122.10	2.35	50.60	1.95	694	9	690	14	694	9
CG-18-02 (75-100)	9277	300.00	13.50	100.10	3.25	34.70	2.15	727	15	696	24	730	15
CG-18-02 (75-100)	9279	246.00	6.50	143.80	3.70	52.50	2.10	624	15	626	13	626	12
CG-18-02 (75-100)	9467	234.00	7.50	178.20	4.85	48.90	2.10	608	14	607	10	607	10
CG-18-02 (75-100)	9467_1	244.00	7.00	176.60	4.25	59.00	2.55	636	13	623	13	629	12
CG-18-02 (75-100)	9498	253.00	5.50	59.50	1.65	64.60	2.00	1999	23	2001	34	1999	23
CG-18-02 (75-100)	9284	242.00	6.00	147.10	3.75	49.10	1.90	645	13	672	14	657	11
CG-18-02 (75-100)	9303	296.00	7.00	219.00	5.50	316.00	13.50	2547	21	2614	56	2526	16
CG-18-02 (75-100)	8627	101.40	2.65	150.40	4.00	163.00	5.00	1872	19	1843	36	1877	18
CG-18-02 (75-100)	8630-30	703.00	23.00	154.00	7.00	104.00	6.50	1712	20	1741	39	1709	19
CG-18-02 (75-100)	8589	1027.00	25.50	1174.00	28.00	329.00	10.50	584	11	583	14	584	11
CG-18-02 (75-100)	8625	174.00	6.00	115.00	2.25	28.30	1.40	609	15	608	14	609	13
CG-18-02 (75-100)	8635	330.00	30.50	264.00	14.00	95.00	11.00	675	14	651	20	675	14
CG-18-02 (75-100)	9527	1047.00	32.50	986.00	20.50	216.00	7.50	599	7	588	15	603	6
CG-18-02 (75-100)	9529	276.00	9.00	262.00	7.50	85.80	3.75	806	15	808	17	807	15
CG-18-02 (75-100)	9616	946.00	29.50	772.00	34.00	199.00	9.50	865	11	817	11	834	11
CG-18-02 (75-100)	9685	479.00	15.50	340.00	11.50	76.20	2.95	606	11	615	13	609	11
CG-18-02 (75-100)	9683	396.00	13.00	216.00	5.00	79.60	2.70	967	9	919	17	995	7
CG-18-02 (75-100)	9676	37.20	0.75	74.50	1.60	23.90	1.00	955	25	820	16	836	16
CG-18-02 (75-100)	9599	592.00	20.50	178.40	4.55	56.60	2.55	802	8	799	15	802	8
CG-18-02 (75-100)	9670	398.00	8.00	191.00	4.75	74.10	2.35	991	10	987	14	991	10
CG-18-02 (75-100)	9669	2990.00	120.00	7900.00	285.00	1910.00	90.00	971	9	877	14	1005	8
CG-18-02 (75-100)	9667	213.80	4.40	240.00	5.50	165.00	6.00	1864	7	1879	17	1863	7
CG-18-02 (75-100)	9656	76.40	1.45	73.80	1.75	26.80	1.25	805	19	854	14	842	13
CG-18-02 (75-100)	8581	302.00	8.00	117.90	2.90	52.70	2.40	975	12	957	15	971	12
CG-18-02 (75-100)	8582-30	267.00	34.50	96.00	10.50	34.00	5.00	780	17	759	26	780	17
CG-18-02 (75-100)	8585	151.70	3.90	102.00	3.80	27.90	1.40	597	15	603	15	600	14
CG-18-02 (75-100)	8618	116.40	4.05	170.00	6.50	66.90	2.70	991	10	992	18	991	10
CG-18-02 (75-100)	8617	171.60	4.95	128.00	4.00	48.30	1.95	749	18	758	17	754	16
CG-18-02 (75-100)	9244	51.60	1.65	81.70	2.75	38.40	1.50	787	19	828	23	798	18
CG-18-02 (100-125)	329	82.10	2.90	64.10	1.85	36.70	2.95	1112	46	616	18	553	18
CG-18-02 (100-125)	229	31.10	1.10	21.80	0.90	7.34	0.46	777	27	599	15	618	15
CG-18-02 (100-125)	244	1270.00	75.00	101.90	4.40	48.70	3.75	691	11	622	10	548	10
CG-18-02 (100-125)	124-1	1790.00	80.00	6810.00	215.00	1780.00	90.00	657	7	567	11	651	7
CG-18-02 (100-125)	124-2	1371.00	49.00	5830.00	195.00	1680.00	75.00	721	13	615	11	640	11
CG-18-02 (100-125)	55-1	1326.00	35.00	5020.00	165.00	1273.00	39.00	686	8	577	8	622	7
CG-18-02 (100-125)	55-2	1454.00	37.00	5990.00	160.00	1439.00	38.00	598	8	519	10	576	9
CG-18-02 (100-125)	6	174.70	3.30	68.80	1.10	20.20	0.60	646	6	600	8	637	6
CG-18-02 (100-125)	442	1146.00	29.00	1250.00	28.50	274.00	13.00	536	5	545	9	536	5
CG-18-02 (100-125)	1683	73.20	2.45	51.20	2.30	25.10	1.45	1152	31	654	14	563	14
CG-18-02 (100-125)	578	234.00	4.85	17.00	0.60	4.57	0.27	808	13	772	14	791	12